Dynamics Simulation of Excited State Intramolecular Proton Transfer

Felix Plasser
Institut für Theoretische Chemie
Universität Wien

Wien, am 26. 3. 2009

Contents

1 Introduction **1**

2 Theory **5**

2.1 The Schrödinger Equation in Chemistry 5

2.1.1 The Born-Oppenheimer Approximation 6

2.2 The Pauli Principle 8

2.3 Dynamics Simulations 9

2.3.1 Classical Dynamics 10

2.3.2 Adiabatic Quantum Dynamics 10

2.3.3 Non-adiabatic Dynamics 11

2.3.4 Analysis of geometry 12

2.4 Computing Electronic Structure 17

2.4.1 General Considerations 17

2.4.2 The Hartree-Fock Method 20

2.4.3 Post Hartree-Fock Methods 21

2.4.4 Density Functional Theory 25

2.4.5 Excited States 27

2.5 Time resolved Experiments 28

3 Computational Considerations **29**

3.1 Dynamics Simulation 29

3.2 Electronic Structure Method 30

3.3 Potential Energy Surfaces 31

3.4 Analysis of Dynamics Simulation 32

4 Results and Discussion **34**

4.1 Stationary points 34

4.2 Potential energy surfaces 39

4.3 Simulated UV spectra 41

4.4 Dynamics Results 41

5 Conclusions and Outlook **49**

Acknowledgements **51**

Deutsche Zusammenfassung **52**

Bibliography **58**

List of Tables **59**

List of Figures **59**

Chapter 1

Introduction

The proton transfer reaction is one of the essential processes in chemistry. It is the main step in the typical (i.e. Arrhenius) acid-base reactions. The properties of liquid water, particularly its conductivity, are governed by the interchange of protons. Deeper understanding of these reactions is important for many processes in technology and biology. But experimental probing is especially challenging because of the short time scale. A fascinating emerging field is concerning the excited state intramolecular proton transfer (ESIPT). Rather than just examining a macroscopic average, a proton transfer along an intramolecular hydrogen-bond is directly triggered with a LASER pulse and probed by a subsequent pulse. Modern femto-second pump-probe techniques allow to follow the reactive process on atomic time and length scales.[1] Today's computational techniques provide very accurate ab-initio treatment of the excited molecules and guide the interpretation of experimentally obtained transients.[2] Aside from the importance of proton transfers for basic research, there are many photo-chemical applications for molecules exhibiting this ESIPT and it may play an important role in photobiology.

The main property that is observed related to ESIPT is a large Stokes shift which comes from the extended excited state relaxation. The absorbed light is typically in the UV and the emission in the visible part of the spectrum unless there is even a radiationless decay to the ground state (cf. Fig. 1.1). In this way the molecule disposes of potentially harmful UV light and works as a photo-

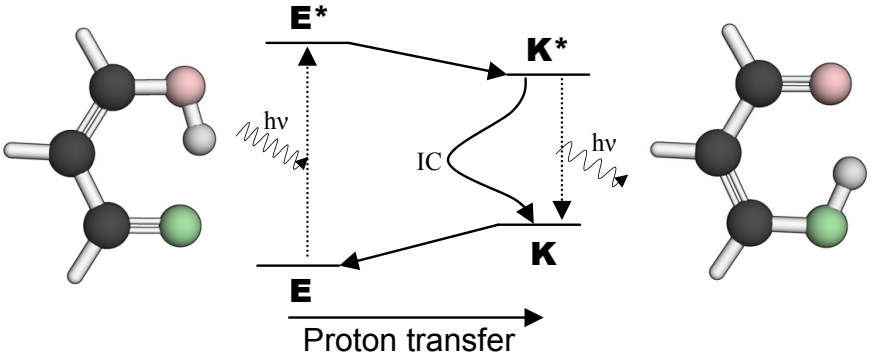

Figure 1.1: *General scheme of ESIPT: The stable tautomer in the ground state (where the hydrogen is often localized on an oxygen) is referred to here as enol (E). After UV excitation the proton transfer to keto (K*) proceeds. K* relaxes either by emitting light with a strong Stokes shift or by internal conversion (IC).*

stabilizer or sun-screen. ESIPT systems are interesting for LASER technology if an excited state tautomer is formed which is not stable in the ground state. This leads to an automatic population inversion independent of the absorption yields. Other ideas are pointed into the direction of control theory[3] and nano-technology, especially molecular switches that are related to the proton transfer and concomitant structural changes[4, 5, 6]. Such switches may be used for data storage or possibly processing. In photobiology excited state proton transfers between the DNA strands may play an important role for excited state relaxation as a protection from photodamage.[7] Proton transfers in photoactive proteins are of great interest as well.[8]

It is a general phenomenon that after photoexcitation a molecule experiences a shift in electron density. This may lead to a change in acid or base constants. If both, the acid and the base centers are located along a hydrogen bond, ESIPT may happen. In many systems this proton transfer is almost barrierless. Then the process occurs on the time scale of a molecular skeletal vibration and the transfer is finished in less than 100 fs. In this context it has to be noted that this ultrafast process is not governed by the hydrogen motion itself but rather by somewhat slower skeletal motions which move the system into a favorable geometry first.[9, 6, 10, 11] If there is a noticeable barrier along the proton transfer

path then usually tunneling plays an important role. In this case the spectra change significantly after deuteration.[12]

In this work the [2,2'-bipyridyl-]-3,3'-diol $BP(OH)_2$ molecule was examined (Fig. 1.2). It is a symmetric (C_{2h}) molecule with two intra-molecular hydrogen bonds. In the ground state the most stable form has the two hydrogens located on the oxygen atoms. This will be called the di-enol (DE) tautomer. A single proton transfer leads to mono-keto (MK), a second one to di-keto (DK). Many experimental[13, 14, 15, 16, 17, 18, 3] and computational[19, 20, 21, 5] studies have been performed on this molecule. From the highly time resolved experiments in connection with computational interpretations the general reaction scheme is known: Within 100 fs after UV excitation DE disappears and and both the MK and DK species are present.[18, 3] Subsequently MK is converted to DK on a 10 ps time-scale.[15] The transfer coherently excites normal modes which keep ringing until well after this time.[3] Then fluorescence from the DK is observed. A quantum yield of 0.22[18] in cyclohexane indicates that it is fairly stable in the excited state. However many other details of this process are not yet known and can only be guessed from the experimental transients. Especially information about the initial transfer step is rather speculative as the time resolution is not quite high enough. A more detailed understanding of the photochemistry of this molecule would be desirable considering many potential applications. They include usage as a LASER dye [13] or a probe in biological systems [22]. Derivatives of $BP(OH)_2$ could be effective photostabilizers or solar energy collectors.[17] The fact that a two channel process is present is interesting in the context of control theory.[3]

The main focus of this work was to get a more detailed insight into the initial transfer step that takes place within 100 fs after photo-excitation[3]. This was achieved by molecular dynamics simulations. Nuclei were considered as classical particles moving in the effective field of the electrons in their first excited state. The electrons were treated quantum mechanically at the ab-initio level. Such an actual numerical solution of the Schrödinger equation even for the excited state has been made possible by the ever increasing speed of computers. The dynamics simulations were supplemented by static calculations to get a more extended view for interpreting the results. The electronic structure methods used in this

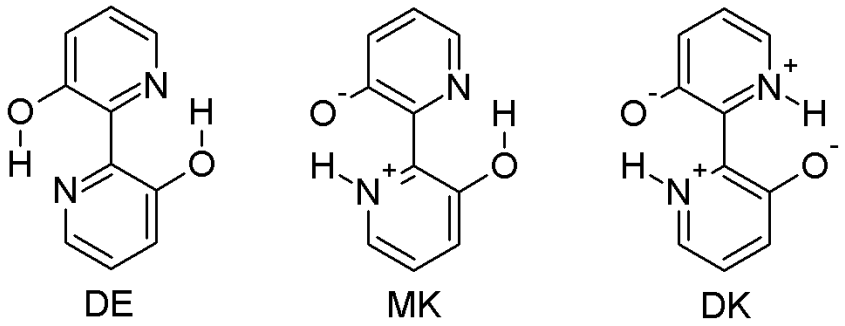

Figure 1.2: *The three tautomers of the [2,2'-bipyridyl-]-3,3'-diol molecule: di-enol (DE), mono-keto (MK), di-keto (DK)*

work were time-dependent density functional theory (TDDFT) and second-order coupled cluster with the resolution of the identity approximation (RI-CC2).

Chapter 2

Theory

2.1 The Schrödinger Equation in Chemistry

In time-independent quantum mechanics the state of a system of N particles is described by its wave function $\Psi(r_1, ..., r_N)$ where $r_i = (x_i, y_i, z_i, \omega_i)$ denotes the three spacial and the spin coordinates of particle i. The physical meaning of the wave function lies in the fact that the probabilty distribution is given by the absolute square of the wave function, i.e. $\Psi(r_1, ..., r_N)^* \Psi(r_1, ..., r_N)$ gives the (differential) probability of find particle 1 at r_1, particle 2 at r_2 etc.

The wave function is found as eigenfunction of the Hamiltonian operator $\widehat{H}$ by solving the Schrödinger equation (2.1). The eigenvalue corresponds to the energy E.

$$\widehat{H}(\Psi) = E\Psi \tag{2.1}$$

The Hamiltonian operator is split up into the kinetic energy operator $\widehat{T}$ and the potential energy operator $\widehat{V}$ (2.2) (where $V(r_1, ..., r_N)$ denotes the potential energy). A stationary solution of the Schrödinger equation corresponds to a constant energy. In this way it is the quantum mechanical equivalent of the energy conservation law.

$$\widehat{H} = \widehat{T} + \widehat{V} \tag{2.2}$$

$$\widehat{T}(\Psi) = \sum_{i=1}^{N} -\frac{\hbar^2}{2m_i} \triangle_i \Psi \tag{2.3}$$

$$\widehat{V}(\Psi) = V(r_1, ..., r_N)\Psi \tag{2.4}$$

$\widehat{T}$ makes up the quantum-mechanical stationary kinetic energy. It is inversely proportional to the mass of the particle m_i. In this way it can be understood that quantum effects become less important when mass increases. Quantum effects are essential for describing electronic behavior. Since the proton is about 2000 times heavier than the electron, quantum effects are less important for atomic nuclei. But it is important to consider zero point vibrations and tunneling phenomena which are especially important for hydrogen, the lightest possible nucleus, and its involvement in proton transfers.

In chemistry atomic units ($\hbar = 1$, $m_{electr.} = 1$, $e = 1$,...) are usually taken to simplify the expression. The considered particles are positively charged nuclei and negatively charged electrons. Let there be N nuclei at positions $(R_1, ..., R_N) = \mathbf{R}$ with charges Z_μ and masses m_μ ($\mu = 1, ..., N$) and n electrons at positions $(r_1, ..., r_n) = \mathbf{r}$. Then the kinetic energy operator can be rewritten according to (2.5). And the potential energy without external influence is given by (2.8).

$$\widehat{T} = \widehat{T}_{nuc} + \widehat{T}_{el} \tag{2.5}$$

$$\widehat{T}_{nuc} = \sum_{\mu=1}^{N} -\frac{1}{2m_\mu} \triangle_\mu \tag{2.6}$$

$$\widehat{T}_{el} = \sum_{i=1}^{n} -\frac{1}{2} \triangle_i \tag{2.7}$$

$$\begin{aligned} V(\mathbf{R}, \mathbf{r}) &= V_{nn}(\mathbf{R}) + V_{ne}(\mathbf{R}, \mathbf{r}) + V_{ee}(\mathbf{r}) := \\ &:= \sum_{\mu=1}^{N-1} \sum_{\nu=\mu+1}^{N} \frac{Z_\mu Z_\nu}{R_{\mu\nu}} - \sum_{\mu=1}^{N} \sum_{i=1}^{n} \frac{Z_\mu}{R_{\mu i}} + \sum_{i=1}^{n-1} \sum_{j=i}^{n} \frac{1}{r_{ij}} \end{aligned} \tag{2.8}$$

It is convenient to rewrite the Hamiltonian according to

$$\widehat{H} = \widehat{T}_{nuc} + \widehat{H}_{el} \tag{2.9}$$

$$\widehat{H}_{el} = \widehat{T}_{el} + \widehat{V} \tag{2.10}$$

2.1.1 The Born-Oppenheimer Approximation

The set of eigenfunctions of $\widehat{H}_{el}$ (defined according to (2.11)) contains an orthonormal basis $\mathcal{B}$, called the adiabatic basis, of the Hilbert space of all possible

wavefunctions $f(\mathbf{R}, \mathbf{r})$.

$$\forall \phi(\mathbf{r}; \mathbf{R}) \in \mathcal{B} : \widehat{H}_{el}(\phi(\mathbf{r}; \mathbf{R})) = E_\phi(\mathbf{R})\phi(\mathbf{r}; \mathbf{R}) \tag{2.11}$$

For the following derivation it is enough to know that this set exists. Finding such functions at fixed nuclear geometries $\mathbf{R}$ is one of the major areas in quantum chemistry. Except for very simple cases only approximative solutions exist and only a few eigenfunctions are computed. Different methods of doing that will be introduced in Section 2.4. The wave function is expressed in terms of these eigenfunctions as an expansion considering all nuclear geometries.

$$\Psi(\mathbf{R}, \mathbf{r}) = \sum_{\phi \in \mathcal{B}} \chi_\phi(\mathbf{R})\phi(\mathbf{r}; \mathbf{R}) \tag{2.12}$$

If (2.12) is plugged into the Schrödinger equation (2.1) with the definition of the Hamilton operator in (2.9) one gets the following result.

$$(\widehat{T}_{nuc} + \widehat{H}_{el} - E)(\sum_{\phi \in \mathcal{B}} \chi_\phi(\mathbf{R})\phi(\mathbf{r}; \mathbf{R})) \equiv 0 \tag{2.13}$$

By applying the scalar product $\langle . \mid . \rangle$ (defined as an integration over all electronic coordinates after taking the complex conjugate of the first expression), equation (2.13) can be rewritten.

$$(2.13) \Leftrightarrow \forall \psi \in \mathcal{B} : \langle \psi | \, (\widehat{T}_{nuc} + \widehat{H}_{el} - E) \sum_{\phi \in \mathcal{B}} \chi_\phi \, | \phi \rangle = 0 \tag{2.14}$$

The three terms corresponding to the three operators can be separately evaluated by considering how the operators act on functions with different arguments.

$$\sum_{\phi \in \mathcal{B}} \langle \psi | \, (-E)\chi_\phi \, | \phi \rangle = -E \sum_{\phi \in \mathcal{B}} \chi_\phi \, \langle \psi \mid \phi \rangle = -E\chi_\psi \tag{2.15}$$

$$\sum_{\phi \in \mathcal{B}} \langle \psi | \, \widehat{H}_{el}\chi_\phi \, | \phi \rangle = \sum_{\phi \in \mathcal{B}} \chi_\phi E_\phi \, \langle \psi \mid \phi \rangle = E_\psi \chi_\psi \tag{2.16}$$

With the kinetic energy operator first the product rule with second derivatives has to be applied (2.18). Then the expression could be rewritten by using the quantum mechanical definition of the momentum as the spatial derivative of the

wave function and then taking the velocity $\mathbf{v}$ (2.19).

$$\sum_{\phi\in\mathcal{B}} \langle\psi|\, \widehat{T}_{nuc}\chi_\phi\, |\phi\rangle = \tag{2.17}$$

$$= \widehat{T}_{nuc}(\chi_\psi) + \sum_{\phi\in\mathcal{B}}(\sum_{\mu=1}^{N} \frac{1}{m_\mu} \bigtriangledown_\mu \chi_\phi \langle\psi|\, \bigtriangledown_\mu |\phi\rangle + \langle\psi|\, \widehat{T}_{nuc}\, |\phi\rangle\, \chi_\phi) = \tag{2.18}$$

$$= \widehat{T}_{nuc}(\chi_\psi) - \sum_{\phi\in\mathcal{B}}(i\mathbf{v}\cdot\langle\psi|\, \bigtriangledown_{\mathbf{R}} |\phi\rangle + \langle\psi|\, \widehat{T}_{nuc}\, |\phi\rangle)\chi_\phi \tag{2.19}$$

With this the Schrödinger equation can be written as (cf. [23]):

$$\forall\psi\in\mathcal{B} : \widehat{T}_{nuc}(\chi_\psi(\mathbf{R}))+E_\psi(\mathbf{R})\chi_\psi(\mathbf{R})-\sum_{\phi\in\mathcal{B}}(i\mathbf{v}\cdot\langle\psi|\bigtriangledown_{\mathbf{R}}|\phi\rangle+\langle\psi|\, \widehat{T}_{nuc}\, |\phi\rangle)\chi_\phi = E\chi_\psi(\mathbf{R}) \tag{2.20}$$

The terms in the sum are called the "non-adiabatic couplings". They are usually very small. Neglecting them reduces (2.20) to isolated equations (2.21). This resembles the Schrödinger equation (2.1) where the potential V is replaced by the electron energy. Nuclei move on an isolated "adiabatic energy surface". This is called the Born-Oppenheimer approximation. Its validity and its exceptions will be discussed in Section 2.3.

$$\widehat{T}_{nuc}(\chi_\psi(\mathbf{R})) + E_\psi(\mathbf{R})\chi_\psi(\mathbf{R}) = E\chi_\psi(\mathbf{R}) \tag{2.21}$$

The significance of this is that the electronic (2.11) and nuclear Schrödinger equations (2.21) can be treated separately. In many cases it is enough to consider the electronic one and consider the nuclei fixed or as classically moving particles. Electronic structure computation will be discussed in Section 2.4.

In a similar way translation and rotation can be separated from the nuclear degrees of freedom. In the general case there are 3 translational and 3 rotational degress of freedom and one only has to consider $3N-6$ internal coordinates (for a linear molecule $3N-5$, for an atom $3N-3=0$).

2.2 The Pauli Principle

A physically valid wave function does not only have to comply with the Schrödinger equation 2.1 but also with the Pauli principle. For electrons (and all other

Fermions) this means that the wave function has to be antisymmetric with regard to the interchange of two electronic coordinates.

$$\phi(r_1, ..., r_i, ..., r_j, ..., r_n) = -\phi(r_1, ..., r_j, ..., r_i, ..., r_n) \tag{2.22}$$

An immediate consequence is that it is not possible that two electrons with the same spin are at the same position (i.e. $r_j = r_i$).

$$\phi(r_1, ..., r_i, ..., r_i, ..., r_n) = -\phi(r_1, ..., r_i, ..., r_i, ..., r_n) \tag{2.23}$$

$$\Rightarrow \phi(r_1, ..., r_i, ..., r_i, ..., r_n) = 0 \tag{2.24}$$

2.3 Dynamics Simulations

Dynamics simulations are concerned with the time-dependent behavior of a system. In this way chemical processes can be directly observed and more information is gained then just by considering the stationary points or other cuts out of the potential energy surface.

In principle the time-dependent Schrödinger equation (2.25) has to be solved.

$$\widehat{H}(\Psi(\mathbf{R}, \mathbf{r}, t)) = i\hbar \frac{\partial}{\partial t} \Psi(\mathbf{R}, \mathbf{r}, t) \tag{2.25}$$

As far as t is concerned this is an ordinary first order differential equation and no eigenvalue problem. The solution (if $\widehat{H}$ is time-independent) is directly given with the time propagator (2.26).

$$\Psi(\mathbf{R}, \mathbf{r}, t) = e^{\frac{it}{\hbar}\widehat{H}} \Psi(\mathbf{R}, \mathbf{r}, t) \tag{2.26}$$

The problem is of course actually evaluating this expression. There are different approximations to this problem. Adiabatic dynamics are run under the assumption of the Born-Oppenheimer approximation (2.21). For non-adiabatic dynamics coupling elements as given in Eqn. 2.19 are evaluated as a post Born-Oppenheimer correction. Another approximation is treating the nuclei as classical particles as far as their kinetic energy is concerned. If this is done with the adiabatic approximation purely classical dynamics result for the nuclei. Non-adiabatic dynamics with classically moving nuclei are called a "mixed quantum-classical" approach.

2.3.1 Classical Dynamics

In the classical limit neither adiabatic quantum effects nor couplings between states are considered (cf. Eqn 2.20). In this way nuclei are classical particles that behave according to Newton's laws. Forces are determined by the gradient of the electronic energy. This leads to a system of coupled differential equations, one for each nucleus.

$$\forall \mu \in \{1, ..., N\} : a_\mu(t) := \frac{d^2}{dt^2} R_\mu(t) = -\frac{1}{m_\mu} \nabla_\mu E_\psi(\mathbf{R}(t)) \tag{2.27}$$

A numerical solution to this is provided by the Verlet algorithm[24] or alternatively if explicit velocity is required the velocity Verlet algorithm. In the second case one starts with a geometry $\mathbf{R}(0)$ and velocity $\mathbf{v}(0)$. The two quantities are propagated according to (2.28) and (2.29) where the acceleration $\mathbf{a}(t) = (a_1(t), ..., a_N(t))$ is computed from the electronic energy gradient (2.27).

$$\mathbf{R}(t + \Delta t) = \mathbf{R}(t) + \mathbf{v}(t)\Delta t + \frac{1}{2}\mathbf{a}(t)\Delta t^2 \tag{2.28}$$

$$\mathbf{v}(t + \Delta t) = \mathbf{v}(t) + \frac{\mathbf{a}(t) + \mathbf{a}(t + \Delta t)}{2}\Delta t \tag{2.29}$$

2.3.2 Adiabatic Quantum Dynamics

Another way to approximate (2.26) is applying the Born-Oppenheimer approximation but retaining other quantum effects. The time-dependent formulation of (2.21) yields (2.30). The solution with a time-independent Hamiltonian is (2.31).

$$\widehat{T}_{nuc}(\chi_\psi(\mathbf{R}, t)) + E_\psi(\mathbf{R})\chi_\psi(\mathbf{R}, t) = i\hbar \frac{\partial}{\partial t} \chi_\psi(\mathbf{R}) \tag{2.30}$$

$$\Leftrightarrow \chi(\mathbf{R}, t) = e^{\frac{it}{\hbar}(\widehat{T}_{nuc} + E_\psi(\mathbf{R}))} \chi(\mathbf{R}, t) \tag{2.31}$$

The major difficulty is evaluating the quantity $E_\psi(\mathbf{R})$. In simple systems like harmonic or Morse oscillators it can be given in analytical form. Usually $E_\psi(\mathbf{R})$ has to be approximated by a grid where at every point an electronic structure calculation (2.11) has to be performed. The number of grid points scales exponentially with the number of degrees of freedom. The problem with large molecules is that most degrees of freedom have to be fixed to reduce the number of grid points. In this way the problem of this approach is that the molecule is constrained in a rather unphysical way.

2.3.3 Non-adiabatic Dynamics

Typically in chemistry the Born-Oppenheimer approximation is valid. But it breaks down when close lying states are present and when nuclear motion is fast (cf. 2.20). In this way non-adiabatic corrections are needed in many cases when excited state dynamics are simulated. The fact that many molecules do not show fluorescence or have a low quantum yield is a clear indicator that the Born-Oppenheimer picture of having two isolated excited states breaks down. The states mix and non-radiative decay takes place. The energy of the excited state is turned into vibrational energy which is subsequently given to the environment. A transition between two states usually occurs close to an intersection, a place where the states are degenerate. But complete degeneracy is not required, the transition takes place because the states are close in energy and the Born-Oppenheimer approximation breaks down.

One way of simulating excited state dynamics is by using the full quantum picture. For this it is convenient to use the diabatic basis. The diabatic basis functions are formed as linear transformations of the adiabatic basis $\mathcal{B}$ (2.11) under the condition that non-adiabatic couplings between the functions are $\mathbf{0}$. With this condition Eqn. (2.20) (and its time-dependent counter part) are greatly simplified. In the next step a model potential may be formed. Then wave packet dynamics may be performed using the multi-configuration time-dependent Hartree method.[23]

An alternative approach are on-the-fly mixed quantum-classical dynamics (MQCD) based on the Surface Hopping method[25] as implemented in our Newton-X molecular dynamics package[26]. Nuclei are treated as classical particles propagated with the velocity-Verlet algorithm (2.28). Then the time-dependent nuclear wave function $\chi_\psi(\mathbf{R}, t)$ is a moving δ-function and can be written as $\chi_\psi(\mathbf{R}(t))$ or as just $\chi_\psi(t)$ a time-dependent coefficient for the adiabatic electronic function $\psi \in \mathcal{B}$. The $\chi_\psi(t)$ (within an adiabatic basis) are propagated according to (2.32) where $\mathcal{B}'$ is the set of states considered.[25] The equation can be seen as a simplification of the time-dependent counterpart of (2.20) where the non-adiabatic coupling arises from the product rule of the spatial derivative. Interestingly the non-adiabatic coupling term can also be obtained as a time derivative of the

moving δ-function[25].

$$i\frac{d}{dt}\chi_\psi(t) + \sum_{\phi\in\mathcal{B}'} i\mathbf{v}(t)\cdot\langle\psi(\mathbf{r};t)\mid\bigtriangledown_{\mathbf{R}}\mid\phi(\mathbf{r};t)\rangle\,\chi_\phi(t) = E_\psi(t)\chi_\psi(t) \tag{2.32}$$

In surface hopping dynamics one initially specifies the states of interest $\mathcal{B}'$. In principle all states have an influence. But this influence is very small if the states are well separated in energy. Therefore typically only the ground state and a few lowest excited states are considered. One also needs a starting state $\phi \in \mathcal{B}'$ and starting geometry and velocity. The dynamics are run by propagating the geometry (2.28) and velocity (2.29) with the velocity Verlet algorithm, and the nuclear wave function coefficients χ_ψ (2.32). For this the gradient of the current state ϕ and the non-adiabatic derivative couplings of ϕ to all other considered states $\psi \in \mathcal{B}'$ are used and have to be computed by the electronic structure program. The complex coefficients χ_ψ do not influence the dynamics directly. The essence of Surface Hopping dynamics is that according to their values stochastic hops to a new state $\psi \in \mathcal{B}'$ are performed and the dynamics continue with the forces of this state.

A similar approach from a practical viewpoint, also leading to on-the-fly dynamcis, is Full Multiple Spawning (FMS)[27]. In FMS the nuclear wave function $\chi_\psi(\mathbf{R},t), \psi \in \mathcal{B}'$ is expressed in a basis of moving Gaussians. For each such basis function, a gradient and non-adiabatic coupling calculation as just described is performed per time step. Then the post Born-Oppenheimer nuclear Schrödinger equation in this basis is solved to get the nuclear wave function coefficients. The basis functions are propagated according to classical forces. In this way an accurate description can be obtained without the need of too many electronic structure computations. To improve the description new basis functions are introduced ("spawned") when needed, typically this is done when the non-adiabatic coupling is large.

2.3.4 Analysis of geometry

A major task in the analysis of dynamics is to reduce the data to find important information. In this work especially geometric parameters were of interest. Two

ways of analyzing them are the use of standard internal coordinates or linear coordinate transformations.

Internal coordinate analysis

Internal coodinates are an alternative to cartesian coordinates when describing a molecular geometry. For a unique description the number of internal coordinates has to be equal to the number of molecular degrees of freedom (typically 3N-6). The most common ones are distances between 2 atoms, bond angles between 3 atoms, and torsion angles between 4 atoms (the angle between the planes spanned by the first three and the last three atoms). The conversion into internal coordinates is performed by geometrical considerations. Well chosen internal coordinates can present a more physical representation of the system. The problem is that the choice of internal coordinates is not unique and that linear dependencies may arise if the structure changes (for example it is not possible to talk about a torsion angle if three of the atoms are in a straight line).

Geometry Superposition

When geometry analysis is carried out in cartesian coordinates proper care has to be taken of translation and rotation. Translation is considered by moving the center of mass to the origin. For rotation structures are aligned by a least squares fit. This can reduce small effects that stem from translation and rotation. A problem is that the fit has discontinuities when the structure changes too much which produces artefacts in some cases.[28]

The weighted root mean square deviation d between two structures $\mathbf{R}$ and $\mathbf{S}$ is defined by equation (2.34). Typically the atomic masses are used for these weighting factors w_α. The RMSD can be seen as a metric in the Hilbert space of nuclear coordinates, it is a weighted norm of the difference vector.

$$W = \sum_{\alpha=1}^{N} w_\alpha \tag{2.33}$$

$$d(\mathbf{R},\mathbf{S}) = \sqrt{\frac{1}{W}\sum_{\mu=1}^{N} w_\alpha \sum_{\alpha\in\{x,y,z\}} (R_{\mu\alpha} - S_{\mu\alpha})^2} \tag{2.34}$$

A rotation $\mathcal{T}$ is applied to a structure by multiplying the coordinates of each atom with a rotation matrix T.

$$\mathcal{T}(R_1, ..., R_N) = (\mathrm{T}R_1, ..., \mathrm{T}R_N) \tag{2.35}$$

The objective of superposition is finding the rotation $\mathcal{T}$ which minimizes the RMSD according to (2.36).

$$d(\mathbf{R}, \mathcal{T}(\mathbf{S})) \rightarrow min \tag{2.36}$$

A convenient way of describing the rotations is through the use of normalized quaternions. Then the RMSD minimization leads to a problem that can be readily solved with Linear Algebra as described in ref. [28]

Normal mode analysis

Normal modes are linear combinations of cartesian coordinates, found as the eigenvectors of the mass-weighted Hessian matrix of the energy. The idea of the normal mode analysis performed in this work was to describe the molecular motion in terms of its normal mode displacements. The coordinate transformation is similar to Ref. [29]. The remaining manipulations that were performed stem from statistical considerations.

Let $\mathrm{Q} = (\mathbf{q_1} \mid ... \mid \mathbf{q_{3N}})$ be the matrix containing the normal modes at a reference geometry in cartesian coordinates and $\mathbf{R}(i,t)$ the cartesian coordinates of trajectory i at time step t. The displacement vector $\mathcal{R}(i,t)$ in normal coordinates with respect to a reference geometry $\mathbf{R}_0$ is found in the following way.

$$\mathcal{R}(i,t) = \mathrm{Q}^{-1}(\mathbf{R}(i,t) - \mathbf{R}_0) \tag{2.37}$$

In a next step one may average over the trajectories to get the motion of the average trajectory $\bar{\mathcal{R}}(t)$. This is shown in equation 2.38 (where n_{Tr} denotes the number of trajectories run in the simulation). $\bar{\mathcal{R}}(t)$ shows coherent activity

present in the dynamics. Only these should remain because with a sufficient sample size random motions should cancel out and the corresponding entries in $\bar{\mathcal{R}}(t)$ should have constant value.

$$\bar{\mathcal{R}}(t) = \frac{1}{n_{Tr}} \sum_{i=1}^{n_{Tr}} \mathcal{R}(i,t) \tag{2.38}$$

To reduce this information one may take the standard deviation over time of this quantity. This leads to a vector $\hat{\mathcal{R}}_{coh}$ that contains one number per normal mode to represent its coherent activity. It is computed as an empirical standard deviation according to (2.39) where k_α and k_ω are the first and last time steps considered and Δt the constant time interval. The value of this quantity represents the coherent activity of a normal mode during the dynamics.

$$\hat{\mathcal{R}}_{coh}^2 = \frac{1}{k_\omega - k_\alpha} \sum_{k=k_\alpha}^{k_\omega} \bar{\mathcal{R}}(k\Delta t)^2 - \left(\frac{1}{k_\omega - k_\alpha} \sum_{k=k_\alpha}^{k_\omega} \bar{\mathcal{R}}(k\Delta t) \right)^2 \tag{2.39}$$

In a similar way the quantity $\hat{\mathcal{R}}_{tot}$ can be defined as the total standard deviation over time steps and trajectories without prior averaging. It should be a measure of the total motion observed along normal modes.

The result does in principle depend on the reference structure $\mathbf{R}_0$ but one could assume that there is no strong dependence as long as a fairly reasonable one is chosen. In the application of this method (cf. Sec. 4.4) it was observed that the results were very similar no matter which one of the equilibrium structures was taken as a reference.

For the application care has to be taken that the description in linear cartesian coordinates is valid. It is problematic once geometric changes are too strong. This was a problem for the test application on retinal analogue "protonated Schiff base 4" (1,3,5-heptatriene-iminium-cation). The hydrogen z-coordinate was H out-of-plane at the starting geometry. But after a rotation around 90° which occured in relation to the non-radiative decay, it constituted a C-H stretch. Hence it was not possible to follow the out-of-plane vibration in this way. A solution may be to use a well chosen set of internal coordinates for the representation of the normal modes.

Essential Dynamics

Another approach for analyzing dynamics motions is called Essential Dynamics (cf. [30]). It is a principal component analysis of the geometric displacements intended to find important motions in the dynamics. This is performed by diagonalizing the covariance matrix. The eigenvectors give the modes of interest, the corresponding eigenvalues represent the variance of these modes.

The two quantities needed to compute the covariance matrix are the vector containing the mean positions $\bar{\mathbf{R}}$ and the $3N \times 3N$ matrix A containing the cross terms, both in cartesian coordinates. In the present case averaging is performed over all trajectories and time steps at once. It would also be possible to compute essential dynamics for an average trajectory but this procedure seems more meaningful as it takes all information that is present.

$$\bar{R}_{\mu\alpha} = \frac{1}{n_{Tr}(k_\omega - k_\alpha + 1)} \sum_{i=1}^{n_{Tr}} \sum_{k=k_\alpha}^{k_\omega} R_{\mu\alpha}(i, k\Delta t) \tag{2.40}$$

$$\mathrm{A}_{\mu\alpha,\nu\beta} = \frac{1}{n_{Tr}(k_\omega - k_\alpha + 1)} \sum_{i=1}^{n_{Tr}} \sum_{k=k_\alpha}^{k_\omega} R_{\mu\alpha}(i, k\Delta t) R_{\nu\beta}(i, k\Delta t) \tag{2.41}$$

$$\mu, \nu \in \{1, ..., N\}; \alpha, \beta \in \{x, y, z\} \tag{2.42}$$

Then the covariance matrix C between the different nuclear coordinates is given according to

$$\mathrm{C}_{\mu\alpha,\nu\beta} = \mathrm{A}_{\mu\alpha,\nu\beta} - \bar{R}_{\mu\alpha}\bar{R}_{\nu\beta} \tag{2.43}$$

Since C is a symmetric matrix it contains a basis of orthogonal eigenvectors $\mathbf{E}_a$. These eigenvectors represent the Essential Dynamics modes. It can be seen that the $\mathbf{E}_a$ are uncorrelated and that the corresponding eigenvalue v_a is the variance of the mode.

$$\mathrm{C}\mathbf{E}_a = v_a \mathbf{E}_a, a \in \{1, ..., 3N\} \tag{2.44}$$

By sorting the $\mathbf{E}_a$ according to their variance v_a important motions can be found. The first piece of information will be found by just viusalizing them. If the modes are fed into the Normal Mode Analysis procedure described above, the time-dependence of the motion can be seen. Alternatively further dynamics simulations including only the first most important modes as degrees of freedom could be carried out.

2.4 Computing Electronic Structure

A major task in quantum chemistry is the computation of eigenfunctions of the electronic Hamiltonian (2.11). In static quantum chemistry parts of the potential energy surface $E_\phi(\mathbf{R})$ (c.f. Eq. 2.11) is constructed. Of special interest are the stationary points, i.e. geometries $\mathbf{R}$ where $\bigtriangledown_{\mathbf{R}} E_\phi(\mathbf{R}) = \mathbf{0}$. In dynamics simulations forces are needed to propagate geometries and velocities (2.28,2.29). Non-adiabatic couplings are needed if non-adiabatic dynamics are performed. Many different approaches to electronic structure theory exist. In any case a compromise between efficiency and accuracy has to be made to provide a good description of the system of interest in reasonable time.

2.4.1 General Considerations

Typically the electronic wave function is expressed in terms of molecular orbitals (MO). An MO $\psi_j(r_i)$ is a function of the coordinates of only one electron. In the simplest case the wave function is expressed as a Hartree product. In this case electrons are statistically independent and have no effect on each other.

$$\phi(\mathbf{r}) = \psi_1(r_1)...\psi_n(r_n) = \prod_{i=1}^{n} \psi_i(r_i) \tag{2.45}$$

A more general form is considering a sum of products.

$$\phi(\mathbf{r}) = \sum_k d_k \prod_{i=1}^{n} \psi_{k(i)}(r_i) \tag{2.46}$$

Slater Determinants

With the general form (2.46) wave functions that comply with the Pauli principle (2.22) can be constructed as "Slater Determinants". Eqn. (2.49) is the explicit definition of the determinant where S_n is the group of permutations and $sgn(\pi)$ is +1 if π is even and -1 if π is odd.

$$\phi_0(\mathbf{r}) = |\psi_1 \dots \psi_n\rangle := \tag{2.47}$$

$$= \frac{1}{\sqrt{n!}} \begin{vmatrix} \psi_1(r_1) & \psi_2(r_1) & \dots & \psi_n(r_1) \\ \psi_1(r_2) & \ddots & & \psi_n(r_2) \\ \vdots & & \ddots & \vdots \\ \psi_1(r_n) & \dots & \dots & \psi_n(r_n) \end{vmatrix} = \tag{2.48}$$

$$= \frac{1}{\sqrt{n!}} \sum_{\pi \in S_n} sgn(\pi) \prod_{i=1}^{n} \psi_{\pi(i)}(r_i) \tag{2.49}$$

Wave functions of this sort are used with the Hartree-Fock method (Section 2.4.2). Post Hartree-Fock methods (Section 2.4.3) consider several determinants.

Second Quantization

An efficient way to deal with Slater determinants that will be used in Sec. 2.4.3 is called Second Quantization. [31] In this approach for each spin-orbital ψ_i a linear annihilation operator $\hat{a}_i$ is defined which removes the spin-orbital ψ_i at the left of a Slater determinant if ψ_i is present in the determinant and sets it equal to $|0\rangle$ if not. In this way an n electron function is transformed into a Slater determinant which depends explicitely only on n-1 electronic coordinate vectors. For applying $\hat{a}_i$, first ψ_i has to be moved to the left position which may change the sign of the determinant (2.50), second the orbital is removed according to the definition of the operator (2.51).

$$\hat{a}_i|\psi_1 \dots \psi_{i-1}\psi_i\psi_{i+1} \dots \psi_n\rangle = (-1)^{i-1}\hat{a}_i|\psi_i\psi_1 \dots \psi_{i-1}\psi_{i+1} \dots \psi_n\rangle := \tag{2.50}$$

$$:= (-1)^{i-1}|\psi_1 \dots \psi_{i-1}\psi_{i+1} \dots \psi_n\rangle \tag{2.51}$$

The adjoint operator of $\hat{a}_i$ is written $\hat{a}_i^\dagger$. According to the definition of an adjoint operator (2.52) $\hat{a}_i^\dagger$ removes an orbital from the bra. (The bra is the vector ready to form a scalar product with a ket or equivalently it could be seen as a linear functional, i.e. an element of the dual space.)

$$\langle\psi_1 \dots \psi_{i-1}\psi_i\psi_{i+1} \dots \psi_n|\hat{a}_i^\dagger := \langle\hat{a}_i(\psi_1 \dots \psi_{i-1}\psi_i\psi_{i+1} \dots \psi_n)| = \tag{2.52}$$

$$= (-1)^{i-1}\langle\psi_1 \dots \psi_{i-1}\psi_{i+1} \dots \psi_n| \tag{2.53}$$

By considering the values of the matrix elements it can be shown that annihilating an orbital in the bra is equivalent to creating an orbital in the ket. Hence $\hat{a}_r^\dagger$ acting on a ket is called the creation operator.

$$\hat{a}_r^\dagger \left|\psi_1 \dots \psi_n\right\rangle = \left|\psi_r \psi_1 \dots \psi_n\right\rangle \tag{2.54}$$

In this way excitations can be conveniently represented. For example the determinant $|\phi_i^r\rangle$ where occupied orbital ψ_i is replaced by unoccupied orbital ψ_r can be written as (2.55).

$$\left|\phi_i^r\right\rangle := \left|\psi_1 \dots \psi_{i-1} \psi_r \psi_{i+1} \dots \psi_n\right\rangle = \hat{a}_r^\dagger \hat{a}_i \left|\phi_0\right\rangle \tag{2.55}$$

The order of the operators is decisive.

$$\begin{aligned} \hat{a}_i \hat{a}_r^\dagger \left|\phi_0\right\rangle &= \hat{a}_i \left|\psi_r \psi_1 \dots \psi_{i-1} \psi_i \psi_{i+1} \dots \psi_n\right\rangle = \\ &= -\hat{a}_i \left|\psi_i \psi_1 \dots \psi_{i-1} \psi_r \psi_{i+1} \dots \psi_n\right\rangle = -\left|\phi_i^r\right\rangle \end{aligned} \tag{2.56}$$

Eqn. (2.56) is an example of the anticommutator relations which can be used to derive the properties of determinants without having to consider their explicit form (2.49), cf. [31].

Basis Sets

The spatial part $\tilde{\psi}(x_i, y_i, z_i)$ of the MOs used to construct the electronic wave function is usually formed as a linear combination of atomic orbitals (AO) $\chi_k(x_i, y_i, z_i)$ (2.57).

$$\tilde{\psi}_i = \sum_k c_{ki} \chi_k \tag{2.57}$$

The χ_k are usually chosen to resemble orbitals in isolated atoms. Slater type orbitals (STO) are more physical and give the correct behaviour including nuclear cusps. But usually Gaussian type orbitals (GTO) are chosen for computational reasons. GTOs can be defined like (2.58) where the radial part is determined by ζ and the angular part by l_x, l_y, l_z [31]. To mimic the behaviour of STOs, linear combinations of GTOs are formed in contracted basis sets. In this way the wave function can be well represented as far as nuclear cusps and also radial nodal

planes are concerned without having the problem of too many independent basis functions.

$$\chi^{GTO}_{\zeta,l_x,l_y,l_z}(r) = N x^{l_x} y^{l_y} z^{l_z} e^{-\zeta r^2} \tag{2.58}$$

Basis sets are classified according to the number and type of basis functions used. A minimal basis set contains a basis function for every atomic orbital in the isolated atom. Multiple ζ basis sets add extra basis functions with the same angular behaviour as in the minimal basis set but with a different prefactor ζ in the exponent. Functions of higher l, called polarization functions, are important for correclty describing bonds. Functions with a small exponent, called diffuse functions, are used to describe long range interactions and are needed for anions and Rydberg states.

2.4.2 The Hartree-Fock Method

In the Hartree-Fock (HF) Ansatz the wave function $\phi_0(\mathbf{r})$ is written as a single Slater determinant (2.47). The HF energy in terms of MO integrals is given according to (2.60) (where integration in the braket is performed over the respective coordinates and $\mathcal{O}$ is the set of occupied orbitals). The expression can be derived by plugging the explicit form of the Slater determinant (2.49) into (2.59) or with the formalism of second quantization (2.4.1).[31, 32]

$$\begin{aligned}
E_0 &= \left\langle \phi_0(\mathbf{r}) \mid \widehat{H}'_{el} \mid \phi_0(\mathbf{r}) \right\rangle := \\
&:= \left\langle \phi_0(\mathbf{r}) \mid \widehat{T}_{el} + V_{ne}(\mathbf{R},\mathbf{r}) + V_{ee}(\mathbf{r}) \mid \phi_0(\mathbf{r}) \right\rangle = && (2.59) \\
&= \sum_{a\in\mathcal{O}} \left\langle a(r_1) \mid -\frac{1}{2}\triangle_1 - \sum_{\mu=1}^{N} \frac{Z_\mu}{R_{\mu 1}} \mid a(r_1) \right\rangle + && (2.60) \\
&+ \frac{1}{2} \sum_{a,b\in\mathcal{O}} \left(\left\langle a(r_1)b(r_2)) \mid \frac{1}{r_{12}} \mid a(r_1)b(r_2) \right\rangle - \left\langle a(r_1)b(r_2) \mid \frac{1}{r_{12}} \mid b(r_1)a(r_2) \right\rangle \right)
\end{aligned}$$

The one-electron terms in (2.60) are the kinetic energy of the electron and the electrostatic interaction between the electron cloud and the nuclei. The first two-electron term is called the Coulomb integral. It gives the average repulsion between the electron clouds and raises the HF energy. The second term, the exchange integral lowering the energy, is a quantum mechanical term that arises

from the antisymmetry of the wave function (c.f. Sec. 2.2). It is non-zero only if a and b are of the same spin. The major source of error in HF theory is that the Coulomb integral overestimates interelectronic repulsion since electrons are unphysically kept from moving out of each others' way. This energy increase is an example of the general fact that according to the variational principle the energy expectation value of any trial function has to be greater or equal to the true ground state energy.

The most common way for solving the HF equations is by expressing the MOs ψ_i as linear combinations of AOs χ_k according to (2.57). This leads to the Roothan-Hall equations. The problem is converted into a non-linear eigenvalue equation which produces the MOs that will give the lowest possible HF energy for the specific basis set.[31, 32] According to the variational principle this should be the best approximation.

2.4.3 Post Hartree-Fock Methods

Several methods have been developed for producing wave functions beyond the Hartree-Fock approximation. The approaches can be grouped into configuration interaction (CI), many-body perturbation theory, and pair theories (most important coupled cluster). But the boundaries between the last two are not clear and different approaches may lead to the same final equations. Moreover combinations can be applied.[31]

Configuration Interaction

In configuration interaction (CI) the wave function is formed as a linear combination of several determinants usually based on a HF reference function (2.61). $\mathcal{O}$ and $\mathcal{U}$ denote the (ordered) sets of occupied and unoccupied orbitals, $\phi_{ab\ldots}^{rs\cdots}(\mathbf{r})$ are the excited determinants where electrons have been moved from orbitals $a, b, \ldots$ to orbitals $r, s, \ldots$. The objective of CI is finding the linear expansion coefficients $d_{ab\ldots}^{rs\cdots}$ which minimize the energy and give the optimal result according to the variation principle. They are found as the lowest energy eigenvector of the CI matrix

which contains the integrals between the different determinants.

$$\phi(\mathbf{r})_{CI} = \phi_0(\mathbf{r}) + \sum_{a\in\mathcal{O}}\sum_{r\in\mathcal{U}} d_a^r \phi_a^r(\mathbf{r}) + \sum_{a<b\in\mathcal{O}}\sum_{r<s\in\mathcal{U}} d_{ab}^{rs}\phi_{ab}^{rs}(\mathbf{r}) + \dots \tag{2.61}$$

Rather than in the basis of Slater determinants, CI may also be performed with configuration state functions (CSF). CSFs are linear combinations of Slater determinants that are already eigenfunctions of the spin operator, i.e. singlets, triplets, etc.

Full CI considers the whole expansion (2.61) which goes until all the electrons are in virtual orbitals. It is the full solution for the Schrödinger equation in a given one electron basis. n_{CI}, the number of considered determinants corresponds to all possibilities of placing n electrons into $|\mathcal{O}|+|\mathcal{U}|$ orbitals. It can be approximately given by (2.62). Hence the method scales exponentially with the electron number.

$$n_{CI} \approx (|\mathcal{O}| + |\mathcal{U}|)^n \tag{2.62}$$

In practice expression (2.61) is usually truncated after a given order, e.g. 2 which leads to CISD. The wave function is variationally determined and hence the energy expectation value is an upper bound of the true gound state energy. But the problem with this approach is lack of size-consistency. This means that any given truncation will recover a larger part of the correlation energy in a smaller system than in a larger one.[31] A way to explain this is to consider for example that CISD is full CI for a two-electron system but truncated CI for a larger system and that there is no reason to assume that the coefficients for higher excitations should be zero. Just for statistical reasons it is expected that higher excitations play a more important role in larger systems. An improvement is the Davidson correction which estimates the effect of quadruple excitations based on the weight of the HF determinant in the expansion.

A variant of the CI approach is the mutli-configuration self consistent field (MC-SCF) method. For a smaller number of determinants orbital coefficients and determinant coefficients are varied simultaneously. A CI computation on top of this is termed multi-reference CI (MR-CI).

Many-body perturbation theory

Another approach for electronic structure calculations is many-body perturbation theory. The method is based on the more general concept of Rayleigh-Schrödinger perturbation theory. In the widely used form called Møller-Plesset perturbation theory (MP) the 0th order Hamiltonian is the HF Hamiltonian $\widehat{H}_0$, defined according to (2.63) where $\hat{f}_i$ is the Fock operator acting on electron i. The perturbation is defined as the difference to the correct Hamiltonian.

$$\widehat{H}_0 = \sum_{i=1}^{n} \hat{f}_i \tag{2.63}$$

The eigenfunctions $\widehat{H}_0$ are all the determinants that can be formed from HF orbitals. Because of this the solutions can be expressed in this basis and no extra differential equations have to be solved. Because of Brillouin's theorem matrix elements between the HF determinant and singly excited determinants are zero. With only one- and two-electron operators also all the matrix elements to triply and higher excited determinants are zero. Therefore only interactions with doubly excited determinants have to be considered.

The 0th order MP energy is the sum of the orbital energies, in 1st order the correct HF energy (2.60) is obtained. The first correction is in the second order leading to the popular MP2 method. According to the considerations above it can be shown that the perturbation energy $E_0^{(2)}$ is given as a quadruple sum over two-electron MO integrals (2.64) where ε_i is the energy of orbital i.[31]

$$E_0^{(2)} = \frac{1}{4} \sum_{\substack{a,b \in \mathcal{O} \\ r,s \in \mathcal{U}}} \frac{\left| \left\langle a(r_1)b(r_2) \mid \frac{1}{r_{12}} \mid r(r_1)s(r_2) - s(r_1)r(r_2) \right\rangle \right|^2}{\varepsilon_a + \varepsilon_b - \varepsilon_r - \varepsilon_s} \tag{2.64}$$

Evaluation of the expression (2.64) can be sped up by using the resolution of the identity (RI) approximation. The idea of this approach is to express the two electron integrals in an auxiliary basis set. The resulting RI-MP2 method cuts down on both computation time and storage needs. Therefore it allows for efficient evaluation of energies, gradients and other properties.[33, 32]

Coupled Cluster Theory

Pair theories consider electron correlation by individual electron pairs. The main representative is coupled cluster (CC) theory. For this it is convenient to define the cluster operator $\hat{\mathcal{T}}^{(m)}$ in the formalism of second quantization (cf. section 2.4.1). The parameters $b_{ab...}^{rs...}$ are called the cluster amplitudes.

$$\hat{\mathcal{T}}^{(m)} = \hat{1} + \hat{\mathcal{T}}_1 + \ldots + \hat{\mathcal{T}}_m \tag{2.65}$$

$$\hat{\mathcal{T}}_1 = \sum_{a\in\mathcal{O}}\sum_{r\in\mathcal{U}} b_a^r \hat{a}_r^\dagger \hat{a}_a \tag{2.66}$$

$$\hat{\mathcal{T}}_2 = \frac{1}{4}\sum_{a,b\in\mathcal{O}}\sum_{r,s\in\mathcal{U}} b_{ab}^{rs}\hat{a}_r^\dagger \hat{a}_s^\dagger \hat{a}_b \hat{a}_a$$

$$\ldots$$

Using $\hat{\mathcal{T}}^{(m)}$ m-th order CI could be expressed according to Eqn. (2.67). In the CC ansatz the exponential of the operator is taken (2.68).

$$\phi(\mathbf{r})_{CI} = \mathcal{T}^{(m)}\phi_0(\mathbf{r}) \tag{2.67}$$

$$\phi(\mathbf{r})_{CC} = \exp(\mathcal{T}^{(m)})\phi_0(\mathbf{r}) \tag{2.68}$$

Through taking the exponential, higher excitations are implicitely considered (2.69) without the need of additional parameters compared to the same order CI.

$$\exp(\mathcal{T}_1) = 1 + \sum_{a\in\mathcal{O}}\sum_{r\in\mathcal{U}} b_a^r \hat{a}_r^\dagger \hat{a}_a + \frac{1}{2}\sum_{a,b\in\mathcal{O}}\sum_{r,s\in\mathcal{U}} b_a^r b_b^s \hat{a}_r^\dagger \hat{a}_s^\dagger \hat{a}_b \hat{a}_a + \ldots \tag{2.69}$$

An advantage of the CC method is that it is size consistent. The CC equations are not solved in a variational approach. This means that the result is not an upper bound of the true energy.

CCS, CCSD, CCSDT, ... denote cluster expansions up to $\mathcal{T}_1, \mathcal{T}_2, \mathcal{T}_3, \ldots$. An approximation to these are the CCS(D), CCSD(T), ... approaches where the last order is treated in a perturbative manner. They are commonly used but not suitable for excited state computation. An alternative approach is in the CC2, CC3, ... series. In the CC2 approach double excitations are approximated whereas single excitations are fully retained. The ground state result is of the same quality as MP2 but the timing is somewhat longer because of the iterative nature. The great advantage of CC2 especially with the RI-approximation is that it allows for excited state computation including come correlation energy on a feasible time scale.[34, 32]

2.4.4 Density Functional Theory

Compared to the wave function based methods just mentioned, density functional theory (DFT) considers only the electron density $\rho(r)$. Whereas a wave function has 3 spatial (+ 1 spin) coordinates for every electron, the density is described by these 3(+1) coordinates only once. This allows for a significant speed up of the procedure.

A functional is a "function of a function" or more precisely a mapping from a vector space into the underlying field. The functional derivative of a functional $A[.]$ at Ψ (if it exists) can be defined as the linear functional $\langle \delta A[\Psi]|$ which fulfills the following relation (2.70).

$$\frac{d}{dt} A[\Psi + t\Phi]_{t=0} = \langle \delta A[\Psi] \mid \Phi \rangle \tag{2.70}$$

In wave mechanics the energy expectation value of a normalized wave function $\Psi(\mathbf{r})$ is given by the functional $E_W[\Psi]$ (2.71). The variation principle (2.72) states that for any given trial function this expectation value is larger than the true ground state energy E_0. Finding the ground state wave function can be considered as a minimization of $E_W[\Psi]$ under the constraint of $\langle \Psi \mid \Psi \rangle = 1$. This is done by searching for a Ψ with a vanishing functional derivative of the Lagrangian (2.73). The Lagrangian parameter E gives the energy expectation value.

$$E_W[\Psi] = \left\langle \Psi \mid \widehat{H}_{el} \mid \Psi \right\rangle, \langle \Psi \mid \Psi \rangle = 1 \tag{2.71}$$

$$\forall \Psi : E_W[\Psi] > E_0 \tag{2.72}$$

$$\langle \delta \left(E_W[\Psi] + E(\langle \Psi \mid \Psi \rangle - 1) \right)| = \langle 0| \tag{2.73}$$

Hohenberg and Kohn [35] showed that similar relations also hold for the density $\rho(r)$. Their first theorem states that for a given stationary electron density there is only one possible external potential. The number of electrons is determined by the integral of the density. Together that means that with a given density the Hamiltonian and hence its lowest eigenvalue, the ground state energy, are clearly determined. Then a functional $E_D[\rho]$ must exist which gives the ground state energy of a given electron density ρ containing n electrons (2.74). The second Hohenberg-Kohn theorem states that there is a variational principle for

the density with a given external potential $v(r)$ (2.75). And again a Lagrangian can be formulated (2.76). The Lagrangian parameter turns out to be the chemical potential μ.[36]

$$E_v[\rho], \int \rho(r) d^3r = n \tag{2.74}$$

$$\forall \rho : E_v[\rho] > E_0 \tag{2.75}$$

$$\left\langle \delta \left(E_v[\rho] + \mu(\int \rho(r) d^3r - n) \right) \right| = \langle 0| \tag{2.76}$$

The difficulty of the DFT approach is that the functional E_v is not known and can only be approximated. It is straight forward to define functionals related to the external potential $V_{ext}[\rho]$ (2.77) and interelectronic Coulomb repulsion of uncorrelated electrons $J[\rho]$ (2.78.[36]

$$V_{ext}[\rho] = \int \rho(r) v(r) d^3r \tag{2.77}$$

$$J[\rho] = \frac{1}{2} \int \int \frac{\rho(r_1)\rho(r_2)}{r_{12}} d^3r_1 d^3r_2 \tag{2.78}$$

An approximation to the kinetic energy can be obtained in the Kohn-Sham formalism [37] which is the most widely used form of DFT. In this approach the wave function is constructed from atomic orbitals $\psi_i(r)$. The single particle kinetic energy is obtained by applying the kinetic energy operator.[38]

$$T_S[\rho] = \sum_{i=1}^{n} \left\langle \psi_i \mid -\frac{1}{2} \triangle \mid \psi_i \right\rangle \tag{2.79}$$

The assumption in Kohn-Sham DFT is that the three terms $V_{ext}[\rho], J[\rho], T_S[\rho]$ should make up the largest part of the energy. The effects that have been neglected are the electron correlation and exchange interactions. These are summarized in the exchange-correlation functional $E_{xc}[\rho]$ and the energy is given according to (2.80).

$$E_v[\rho] = V_{ext}[\rho] + J[\rho] + T_S[\rho] + E_{xc}[\rho] \tag{2.80}$$

So far no approximations have been made but the problem with the approach is that E_{xc} is not known. An early parametrization that uses only local information is the local density approximation. It is mainly used in solid state chemistry. The generalized gradient approximation also includes the gradient of the density

in the computation. One prominent representative, the PBE functional gives good results in both solid state and molecular chemistry. A different approach is computing the Hartree-Fock exchange (cf. Eqn. 2.60) of the Kohn-Sham orbitals and including a fraction of this into the functional. These hybrid functionals, like B3LYP, are very popular in molecular computations.[38]

2.4.5 Excited States

Electronically excited states are eigenfunctions of $\widehat{H}_{el}$ other than the ground state. They are used to describe a molecule after UV excitation or higher energy irradiation. Excited state computation can be divided into direct and propagator approaches.[2]

In CI based methods excited states are found directly as higher energy eigenvectors of the CI matrix. The minimal version CIS gives a qualitative picture of excited states but lacks electron correlation which can be crucial for the correct state order and excitation energies. In the state-averaged MC-SCF formalism orbitals are optimized for each excited state considered which improves the result and allows for accurate treatment of multi-configurational character. Improvement of MC-SCF results with MR-CISD gives very accurate energies but is only feasible for small molecules. An alternative approach of improving the MC-SCF result is multi-reference perturbation theory which works similar to MP2.[39]

Excitation energies can be obtained without explicit construction of the excited state wave function from the frequency dependent ground state polarizability. This gives rise to the time-dependent DFT (TDDFT) method which is popular because it produces high level results at a low cost.[40] Linear response CC2 [34, 32] produces good results for excited states and is still rather efficient. If more accurate results are required, CCSD excitation energies can be obtained with the equation-of-motion formalism.[2]

2.5 Time resolved Experiments

In the recent years experimental time resolution has been extended into the femto second regime. The main step was the production of the corresponding LASER pulses. A sub-picosecond pulse is split up with a semi-transparent mirror and sent along two paths of slightly different lenghts, e.g. a difference of 0.3 mm leads to a 1 ps delay. The pump pulse is the one with the slightly shorter path and reaches the sample at equilibrium. The probe pulse which has a slight delay is used to measure the process. Different methodologies for the measurement exist. The second pulse may cause stimulated emission which can be detected. In resonant multi-photon ionization the second pulse leads to ionization of the sample. The formed ions can be detected by mass spectrometry.[41] In transient photo-electron spectroscopy the energy of the emitted electrons is measured. An alternative option is fluorescence upconversion.[18] High quality results are obtained if spectroscopy is performed in an ultrasonic beam. This jet cooling leads to vibrationally relaxed molecules which gives the possibility for obtaining extra information.[41]

From the wave number $\bar{\nu}$ of a normal mode, the oscillation period T is obtained according to (2.81). For example a 200/cm normal mode has an oscillation period of 167 fs which is well above the time-resolution that can be achieved. That means that actual atomic motions can be probed. One of the first systems where the oscillations were directly observed was the $I-Hg-I$ molecule because the heavy atoms result in a low vibration/excitation frequency. Today also skeletal modes in regular organic molecules are seen.[1]

$$T = \frac{1}{\bar{\nu}c} \tag{2.81}$$

The maximum uniquely determined frequency in discrete Fourier analysis amounts to half of the sampling frequency. Using Eqn. (2.81) the maximum probed wave number can be easily computed. For example a 30 fs sampling frequency corresponds to a maximum accessed wave number of 556/cm.

Chapter 3

Computational Considerations

The aim of this study was the simulation of the excited state behaviour of the [2,2'-Bipyridyl-]-3,3'-diol ($BP(OH)_2$) molecule. It is known from experiments and earlier computations that the molecule exhibits single and double proton transfer after UV excitation along intramolecular hydrogen bonds. In the ground state the di-enol (DE) structure where both hydrogens are bound to oxygens is stable. In the excited state one or two protons are transferred to yield mono-keto (MK) or di-keto (DK) respectively.

3.1 Dynamics Simulation

$BP(OH)_2$ has a considerable quantum yield of 0.22 [18]. Only one study reported possible ground state decay which was expected to occur at a time scale of 20 ps [16]. This means that decay to the ground state is expected to be negligible within the 100 fs simulated. Moreover the important part of the dynamics should occur in the $\pi\pi^*$-state which is the first excited state at the Franck-Condon point. $n\pi^*$ influence was described in Ref. [16] but it should only play a minor role. In this way adiabatic dynamics on a sinlge state can be performed.

The next question is wether adiabatic quantum dynamics (cf. Eqn. 2.31) have to be performed or if nuclei can be treated as classical particles. Generally it is established by experiment and computation that hydrogen tunneling may play a

role in excited state proton transfer processes with both intermolecular [42, 43] [44] and even intramolecular [12] proton transfer. But if no barrier is present there is no need for tunneling and the transfer proceeds on the time scale of skeletal normal modes in less than 100 fs [10, 11]. For $BP(OH)_2$ it was shown that the transfer is not affected by substitution of the hydrogen atoms against deuterium [45]. According to the definition of the kinetic energy operator (2.3) a change in mass should strongly affect a tunneling process (cf. examples in Ref. [42]). This is a clear indicator that tunneling should not play a role in this case.

Neither non-adiabatic nor adiabatic quantum effects are expected to play a role in the process. Therefore the simulations were performed using classical dynamics for the nuclei (cf. Sec. 2.3.1). Only with initial condition sampling quantum mechanics were taken into account. Both, initial nuclei positions and momenta were chosen considering the zero point vibrations according to the Wigner distribution, cf. [26]. In the course of the dynamics positions and momenta were updated according to the velocity Verlet algorithm (2.28, 2.29) with a time step of 0.5 fs. At the TDDFT level 100 trajectories were computed up to 100 fs. Due to increased computer time only 36 trajectoreis up to 100 fs were computed at the RI-CC2 level. To get some more insight on the later steps, 11 trajectories were extended up to 300 fs.

3.2 Electronic Structure Method

As mentioned above (section 3.1) decay to the ground state is not expected to occur within the 100 fs simulated. Moreover no significant geometric changes are expected during the process. Because of this it should suffice to use a single reference method.

The size of the system (14 heavy atoms and 8 hydrogens) allows for ab-initio treatment of the electronic structure even in the excited state. Two feasible approaches for this are the time-dependent density functional theory (TDDFT, Sec. 2.4.4) [46, 47, 40] and second-order approximate coupled cluster [34] with the resolution of the identity approximation for 2-electron integrals (RI-CC2) [48, 49, 32] (cf. Sec. 2.4.3). For TDDFT the B3LYP [50] functional has been

taken whose suitability for excited state proton transfer has been shown in Ref. [51]. For all electronic structure computations the Turbomole program package [52] was used.

Two basis sets were used in the simulations, the TZVP [53] basis set and a mixture of SVP and SV [54] which will be called "SVP-SV". The TZVP basis set has triple-ζ quality valence orbitals with polarisation functions. For heavy atoms it contains 5 s-exponents, 3 p-exponents, and 1 d-exponent. This leads to 19 basis functions considering the degeneracy of the p- and d-orbitals. 3 s-, and 1 p-exponents lead to 6 functions for hydrogen. In total 314 contracted basis functions were considered. The "SVP-SV" basis set consisted of SVP (double-ζ ("split") valence polarization) for heavy atoms (3s 2p 1d) and polar hydrogens (2s 1p) and SV (split valence) for hydrogens bonded to carbon (2s). In total this lead to 218 contracted basis functions.

Dynamics and spectra simulations were performed with the SVP-SV basis set with the RI-CC2 and TDDFT/B3LYP methods. Geometry optimizations were perforemd at the TDDFT/B3LYP/SVP-SV, TDDFT/B3LYP/TZVP, and RI-CC2/SVP-SV levels. RI-CC2/TZVP was used to compute single point energies on the RI-CC2/SVP-SV structures.

3.3 Potential Energy Surfaces

The quantity $E_\phi(\mathbf{R})$, i.e. the potential energy acting on the nuclei for electrons in state ϕ (cf. Eqn. 2.11), is a multidimensional function depending on all the nuclear degrees of freedom $\mathbf{R}$. To represent it in an efficient way usually potential energy surfaces (PES) are computed by only varying a few important degrees of freedom. Two kinds of 2-dimensional PES's have been computed in this study, one with a relaxed geometry and one with structures obtained from linear interpolation.

The idea of a reaction coordinate driven PES is to change an internal coordinate which is expected to be important in the reaction and relax the remaining structure. An advantage of this approach is that the resulting surface contains the

stationary points. For $BP(OH)_2$ this has been performed by setting the two OH distances to different values and optimizing the remaining geometric parameters.

Additionally a grid with linear interpolation was computed. This was done in a similar way to Ref. [21]. The ground state FC minimum $\mathbf{R}_{FC}$, the two mirrored $\pi\pi^*$ MK minima (under planarity restriction) $\mathbf{R}_{MK_1}, \mathbf{R}_{MK_2}$, and the $\pi\pi^*$ DK minimum $\mathbf{R}_{DK}$ were used. A linear interpolated structure $\mathbf{R}(\xi_1, \xi_2)$ was formed according to (3.1) and the corresponding single point energy was computed.

$$\begin{aligned} \mathbf{R}_0 &= \frac{1}{4}(\mathbf{R}_{FC} + \mathbf{R}_{MK_1} + \mathbf{R}_{MK_2} + \mathbf{R}_{DK}) \\ \mathbf{R}(\xi_1, \xi_2) &= \mathbf{R}_0 + \xi_1(\mathbf{R}_{DK} - \mathbf{R}_{FC}) + \xi_2(\mathbf{R}_{MK_2} - \mathbf{R}_{MK_1}) \end{aligned} \tag{3.1}$$

In the original work [21] a similar grid based on the ground state structures was computed because through this optimizations in the excited states could be avoided. Another advantage is that in this linear approach clear effective masses can be assigned to the degrees of freedom which allows for quantum mechanical wave packet propagation. The downside is that neither of the stationary points is actually on the surface. In total it seems that the first kind of surface is more useful unless one wants to avoid excited state geometry optimizations.

3.4 Analysis of Dynamics Simulation

The analysis of the dynamics was mainly concerned with geometric changes as the process of interest was a geometric change rather than a change in electronic structure. The three methods described in Section 2.3.4 were used. Internal coordinate analysis was readily available as part of the Newton-X package [26]. Distances of the H atom to the O and N atoms on either side ($R_{OH,1}, R_{OH,2}, R_{HN,1}, R_{HN,2}$) were chosen to represent the hydrogen transfer process. The distances between the O and N atoms ($R_{ON,1}, R_{ON,2}$) should show skeletal geometric changes. For further analysis a reaction coordinate was defined according to (3.2).

$$\Delta R_i = R_{OH,i} - R_{HN,i}; i \in \{1, 2\} \tag{3.2}$$

In this way a proton transfer on side i could be defined as the point in time when $\Delta R_i = 0$, and the tautomer structures according to (3.3-3.5). The *active* side

was defined as the side of the first proton transfer.

$$DE \Leftrightarrow \Delta R_1, \Delta R_2 \leq 0 \tag{3.3}$$

$$MK \Leftrightarrow (\Delta R_1 \leq 0 \wedge \Delta R_2 > 0) \vee (\Delta R_1 > 0 \wedge \Delta R_2 \leq 0) \tag{3.4}$$

$$DK \Leftrightarrow \Delta R_1, \Delta R_2 > 0 \tag{3.5}$$

Normal mode analysis (Sec. 2.3.4) and Essential Dynamics (Sec. 2.3.4) were performed. To do this, first an alignment of the structures (Sec. 2.3.4) had to performed. There was no code available for this and the manipulations described had to be implemented. This was done with the Python programming language. Linear algebra manipulations were performed with the numpy Python package. For manipulation of chemical structure files the openbabel package was used. The routines developed in this work will be implemented into the Newton-X molecular dynamics package[26].

Geometry alignment was done according to a least squares fit. The procedures were coded in Python according to the prescript given in Ref. [28]. A difficulty in the current project was the breaking of symmetry that went along with the single proton transfer. In order to account for this, in all the trajectories the active side was identified and the atoms renumbered to have it on the same side of the molecule. After this the structures were superposed on the DK minimum. On these aligned trajectories the algebra of normal mode analysis and essential dynamics was carried out. In the case of normal mode analysis the absolute value of the displacement $\mathcal{R}(i,t)$ was taken for out-of-plane modes as the motion in both directions is equivalent.

Chapter 4

Results and Discussion

In this section the results of the computations will be presented. They have been published in Refs [55] and [56]. Here the important results will be reviewed and some complimentary information will be given.

4.1 Stationary points

Six stationary point structures were considered in the study. The three energy minima corresponded to the structures of interest: the di-enol (DE), the mono-keto (MK), and the di-keto (DK). Two first order saddle points were computed to give the transition states between DE-MK and MK-DK. A second order saddle point represented the symmetric transfer DE-DK. The geometries of the minima can be seen in Figure 4.1. Except for the DE ground state all other structures are computed for the excited $\pi\pi^*$ state. The RI-CC2/SVP-SV and TDDFT/B3LYP/TZVP results will be discussed, TDDFT values in parentheses. The LUMO in the symmetric tautomers is delocalized over the inter-ring CC bond (cf. Ref. [20]), whose distance is shortened by 0.06 Å (0.06 Å) on excitation. It can be seen through shortening of the CO distance by 0.04 Å (0.07 Å) that the keto functionality is formed. A similar shortening was observed in the HBT molecule.[11] In the MK tautomer the interring CC distance remains unchanged with RI-CC2 and increases by 0.04 Å with TDDFT. In this structure the HOMO

Table 4.1: *Lengths of the hydrogen bonds computed with different methods. Optimizations were done with C_s restriction. FC denotes Franck-Condon structure, i.e. the ground state DE. MK and DK are optimized in the $S_1(\pi\pi^*)$ state.*

Method	FC (N···H)	MK (N···H)	MK (O···H)	DK (O···H)
B3LYP/SVP-SV	1.658	1.741	1.751	1.696
B3LYP/TZVP	1.686	1.777	1.783	1.722
RI-CC2/SVP-SV	1.638	1.615	1.744	1.667
RI-CC2/TZVP	1.645	1.621	1.755	1.671

and LUMO are localized on different rings. Keto formation reduces the CO bond by 0.02 Å (0.07 Å). With RI-CC2, a shortening of the N···H hydrogen bond by 0.02 Å is observed, while its length increases by 0.09 Å at the TDDFT level.

Because of weaker interaction energies and flatter potentials hydrogen bonds are rather sensitive to the computational description. This could also be seen in this sudy. To allow for a closer comparison between methods, hydrogen bond lengths. of structures with planarity restriction at different levels of theory are summarized in Table 4.1. Values computed with the RI-CC2 method are significantly smaller than those obtained at the (TD)DFT level. This effect amounts to about 0.02-0.04 in the electronic ground state and increases to above 0.1 for the N···H bond length in the MK structure in the S_1 state. A similar trend with similar numbers was also seen in our previous study [51]. The absence of an excited state DE minimum at the RI-CC2 level and the smaller MK-DK barrier could be explained by the presence of stronger hydrogen bonds in this method. The hydrogen bond lengths increase when a larger basis set is used which is probably related to a decrease in the basis set superposition error which is known to overstabilize such interactions. The effect is strong at the DFT level and hardly noticable with RI-CC2.

The relative energies of the structures are shown in Fig. 4.2. At the RI-CC2 level vertical excitation amounts to 3.901 eV. The Franck-Condon excited structure relaxes without a barrier to either the MK or DK forms which are about equal in energy. The MK→DK reaction barrier amounts to 0.126 eV. At the TDDFT level there exists a shallow DE minimum with a very low barrier (0.002 eV) toward

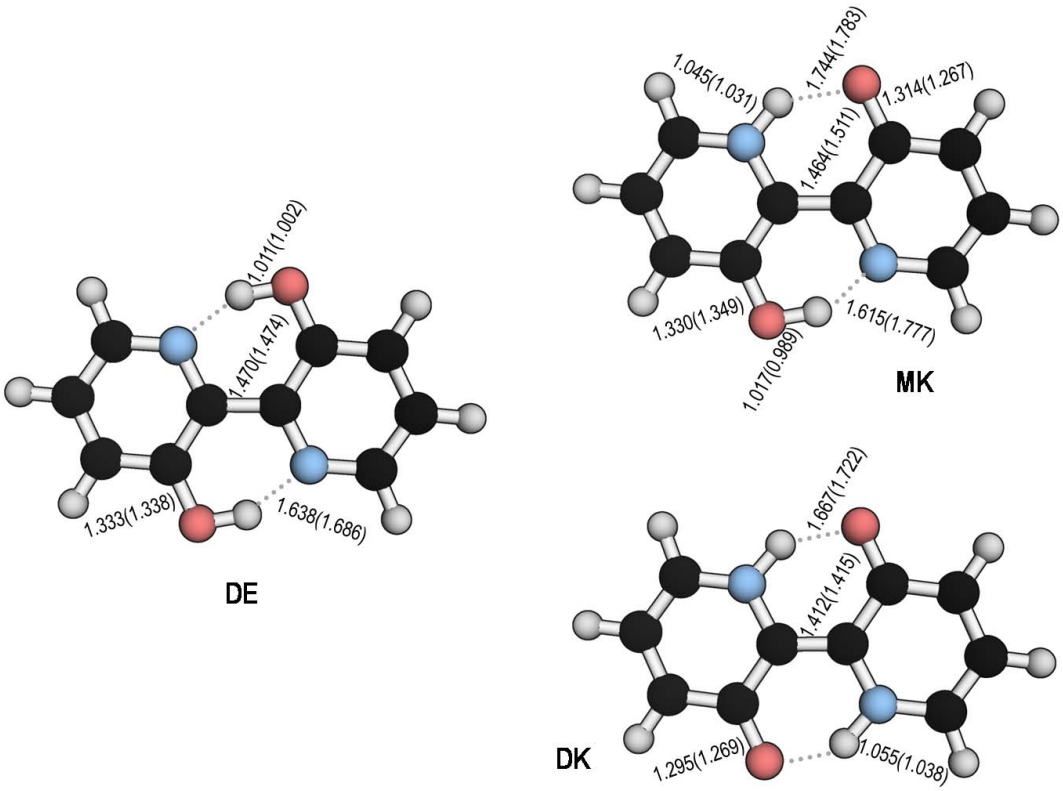

Figure 4.1: *Ground state (DE) and S_1 ($\pi\pi^*$) state (MK, DK) fully optimized geometries at the RI-CC2/SVP-SV level. (TD)DFT/B3LYP/TZVP values are shown in parentheses; at the MK the TDDFT/B3LYP/TZVP structure with planarity restriction is taken as no true local MK minimum was found. For DE and DK only symmetry unique values are shown. DE and DK are planar, MK shows an NCCN interring torsion angle of 175°.*

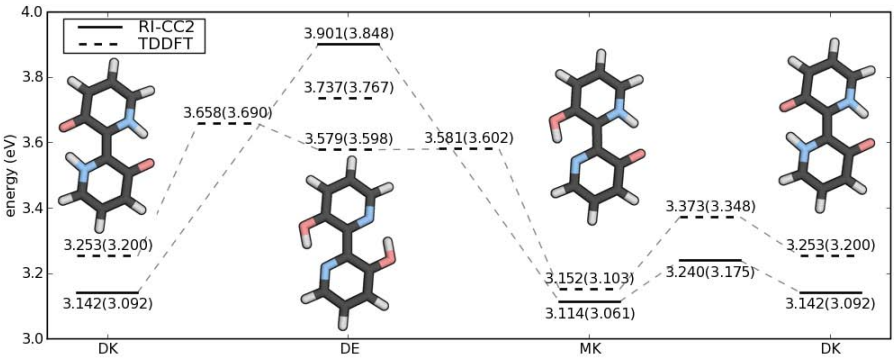

Figure 4.2: *S_1 ($\pi\pi^*$) energies for planar structures relative to the DE ground state minimum computed at the RI-CC2 and TDDFT/B3LYP levels using the SVP-SV and TZVP basis sets, TZVP results in parentheses.*

MK formation. Symmetric DK formation would proceed over a second order saddle point with a barrier of 0.079 eV. In TDDFT MK is considerably more stable (0.101 eV) than DK. And the MK→DK barrier (0.221 eV) is about twice as high as with RI-CC2.

Vertical excitation energies for the first 7 states at the DE ground state minimum are shown in Table 4.2. The most intense transition is to the S_1 ($\pi\pi^*$) state which can be characterized as a HOMO-LUMO excitation. Because of the high oscillator strength mostly this state will be accessed by the experiment. The excitation energy computed here is quite similar to the experimental absorption maximum of 3.647 eV[14] measured in cyclohexane. The fact that the energy is a little bit too high may be related to solvation effects. Several states of $\pi\pi^*$ (A_g, B_u) and $n\pi^*$ (A_u, B_g) character are following S_1 and have zero or small oscillator strength. The next state with larger oscillator strength is the $2^1\mathrm{B_u}$ state which is S_5 at TDDFT and S_6 at RI-CC2, respectively. This may be the origin of the second peak in the absorption spectrum reported below 250 nm [14, 15]. It may also be the doorway state for experiments with excitation at 267 nm. The significance of this is that at 267 nm different dynamics take place. With this higher excitation energy a transient MK/DK ratio of 2:1 is seen rather than the DK excess seen at lower excitation energies.[14, 15, 3] No further examinations on this question have been made. It can be seen that the RI-CC2 excitation energies are generally

Table 4.2: *Vertical excitation and fluorescence energies (eV) of the first singlet excited states computed at different levels of theory. Oscillator strengths are shown in parentheses.*

	TDDFT/B3LYP			RI-CC2			Exp.[a]
Struct.	State	SVP-SV	TZVP	State	SVP-SV	TZVP	
FC	1^1B_u	3.737(3.38E-01)	3.767(3.49E-01)	1^1B_u	3.901 (3.75E-01)	3.848 (3.73E-01)	3.647
FC	1^1A_u	4.305 (1.45E-03)	4.362 (2.62E-03)	2^1A_g	4.685 (0)	4.607 (0)	
FC	2^1A_g	4.559 (0))	4.552 (0)	1^1A_u	4.686 (1.51E-03)	4.662 (1.66E-03)	
FC	3^1A_g	4.668 (0)	4.658 (0)	3^1A_g	5.402 (0)	5.280 (0)	
FC	2^1B_u	5.057 (5.83E-02)	5.041 (5.96E-02)	1^1B_g	5.506 (0)	5.454 (0)	
FC	1^1B_g	5.143 (0)	5.124 (0)	2^1B_u	5.618 (9.44E-02)	5.493 (1.03E-01)	
FC	2^1B_g	5.462 (0)	5.443 (0)	2^1B_g	5.960 (0)	5.873 (0)	
MK	2^1B_u	2.466 (1.48E-01)	2.409 (1.47E-01)	2^1B_u	2.488 (3.11E-01)	2.477 (2.73E-01)	2.183
DK	2^1B_u	2.708 (3.40E-01)	2.690 (3.63E-01)	2^1B_u	2.599 (3.98E-01)	2.583 (4.27E-01)	2.431

[a]Ref. [14]

somewhat higher than the TDDFT results. Basis set dependence is rather small. With RI-CC2 both the two A_g and B_g states have multi-reference character and mixing between them may not be appropriately described. But for the states of interest the approach should be accurate. Also the vertical fluorescence energies and corresponding oscillator strenghts of the MK and DK structures are shown in Table 4.2. Similar values to the experiment and most importantly the same ordering are obtained. This is a verification of the respective assignment of the experimental bands to the MK and DK structures.

There is a rather large gap to the first $n\pi^*$ state (1^1A_u) of about 0.6 eV in the Franck-Condon region. At this geometry an electron is taken out of a non-bonding orbital of a nitrogen atom. The situtation drastically changes after one or two protons are transferred and the non-bonding orbital is supplied by an oxygen atom. At MK and DK type geometries the $n\pi^*$ state becomes competitive with $\pi\pi^*$ and true S_1 minima exist where this S_1 state is of $n\pi^*$ character. Their energies are very similar to the ones of the $\pi\pi^*$ minima.

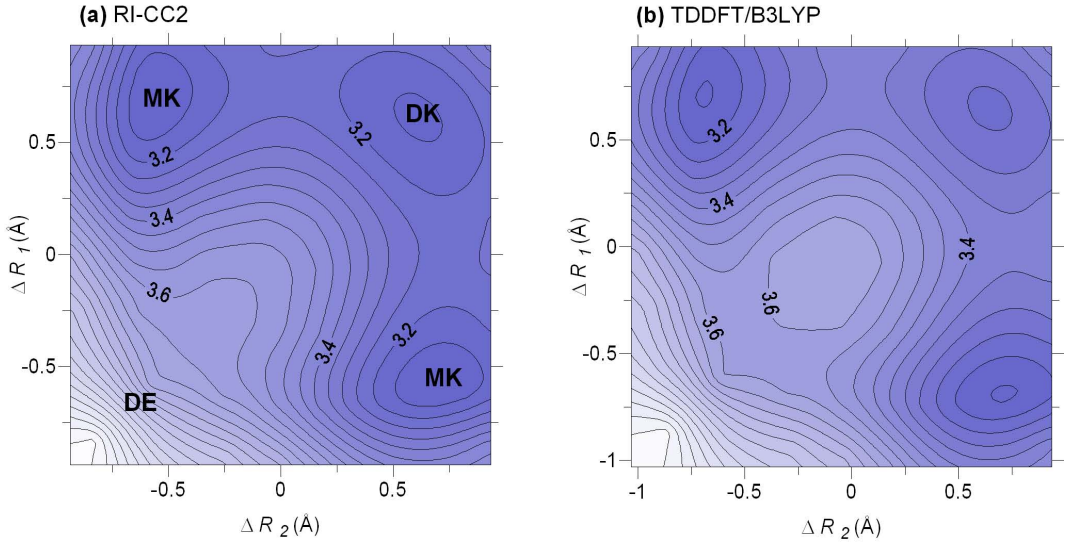

Figure 4.3: *Relaxed PES with fixed OH-distances under planarity constriction in the $\pi\pi^*$ state computed at the RI-CC2/SVP-SV (a) and TDDFT/B3LYP/SVP (b) levels.*

4.2 Potential energy surfaces

Two-dimensional potential energy surfaces have been computed by fixing the two OH-distances at different values and relaxing the remaining structure under planarity constriction. This is intended to give insights into the reaction dynamics. But it should be remembered that in the sub 100 fs process considered it cannot be expected that the geometry relaxes fully. This means that the dynamics do not actually proceed on this PES but rather above it as far as the energy is concerned. The advantage of the approach is that the stationary points of interest are part of such a surface. In this way surfaces at the RI-CC2/SVP-SV and B3LYP/SVP level have been computed for the $\pi\pi^*$ state (Fig. 4.3).

In the Franck-Condon region (i.e. close to the DE structure) both surfaces show a steep decline. On the other side wells for the MK and DK structures are found. The symmetric DE→DK path proceeds over an elongated shallow area in RI-CC2. In TDDFT there is even a second order saddle point in the way and a shallow DE minimum exists (cf. Fig. 4.2). In both cases the symmetric transfer seems rather unlikely as the symmetric path forms a ridge which is unstable toward

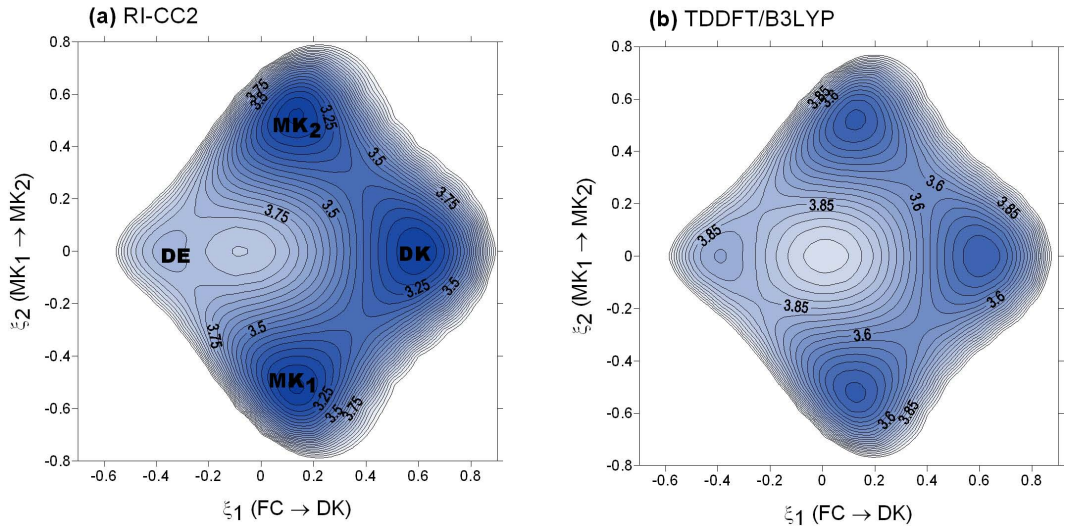

Figure 4.4: *Linear PES computed at the RI-CC2/TZVP (a) and TDDFT/B3LYP/TZVP (b) levels. The structures were constructed according to (3.1).*

unsymmetric MK formation. Only highly symmetric starting conditions would lead to a symmetric double proton transfer and symmetry breaking is expected by considering these PES's. For the geometries considered in the PES's also vertical energies of the $n\pi^*$ state have been considered. The shape of this PES is rather similar and dynamics in this state should proceed in a similar way. An important fact is that the $n\pi^*$ energies are very close to the $\pi\pi^*$ energies even for structures optimized at the $n\pi^*$ level. As mentioned above (Sec. 4.1) true minima for $n\pi^*$ as the first excited state exist.

For comparison with a quantum dynamical study that has been recently performed [21] also a linear PES has been constructed (Fig. 4.4). Contrary to the study mentioned, the MK and DK structures optimized in the excited ($\pi\pi^*$) state have been taken. The definition of structures was according to (3.1). And single point calculations with the TZVP basis set have been performed.

In general the linear PES's are very similar to the relaxed PES's. MK and DK wells are clearly seen. A difference is that in the linear grid even RI-CC2 shows a shallow DE minimum and the corresponding second order saddle point.

4.3 Simulated UV spectra

For a more accurate comparison with experimental results, UV spectra were simulated. This is done by doing single point calculations on random structures created by a Wigner distribution in the same way as for the initial conditions generation of the dynamics (Sec. 3.1). The results for RI-CC2/SVP-SV and B3LYP/SVP-SV are shown in Fig. 4.5. In this figure the large Stokes shift that goes along with the extensive excited state relaxation caused by the proton transfer can be clearly seen. For the Franck-Condon absorption and DK fluorescence, the results are very similar: absorption in the near UV and green fluorescence as is also known from experiment. Even the shoulder to the right of the maximum in the experimental spectrum [14] is well reproduced. For MK RI-CC2 shows the behavior that is expected from experiment: a fluorescence band slightly red-shifted compared to DK. In B3LYP the vertical fluorescence from MK with planarity restriction is also good. But the MK band in the simulated spectrum is stretched to lower energies. This has to do with the fact that after inter-ring torsion there is a clear charge transfer state in the MK. And it is a well known fact that standard density functionals are not suitable for describing charge transfer states.[2] In Figure 4.5 it can also be seen that the band maxima are always slightly red-shifted compared to the vertical excitations. The RI-CC2 band maxima are always slightly higher in energy than the experimental values, with B3LYP the absorption maximum is very close to, DK higher and MK lower in energy than the experimental value. An important result of this calculation is that the ordering is consistent with the experimental interpretion of the bands, i.e. DK at 510 nm and MK at 568 nm.

4.4 Dynamics Results

Dynamics simulations were performed to get a direct insight into the process. In the computed PES (Fig. 4.3) it can be seen that there is a barrierless asymmetric one-proton-transfer-path leading to the MK. The symmetric path is also barrierless in RI-CC2 and has a second order saddle point in TDDFT/B3LYP. But in

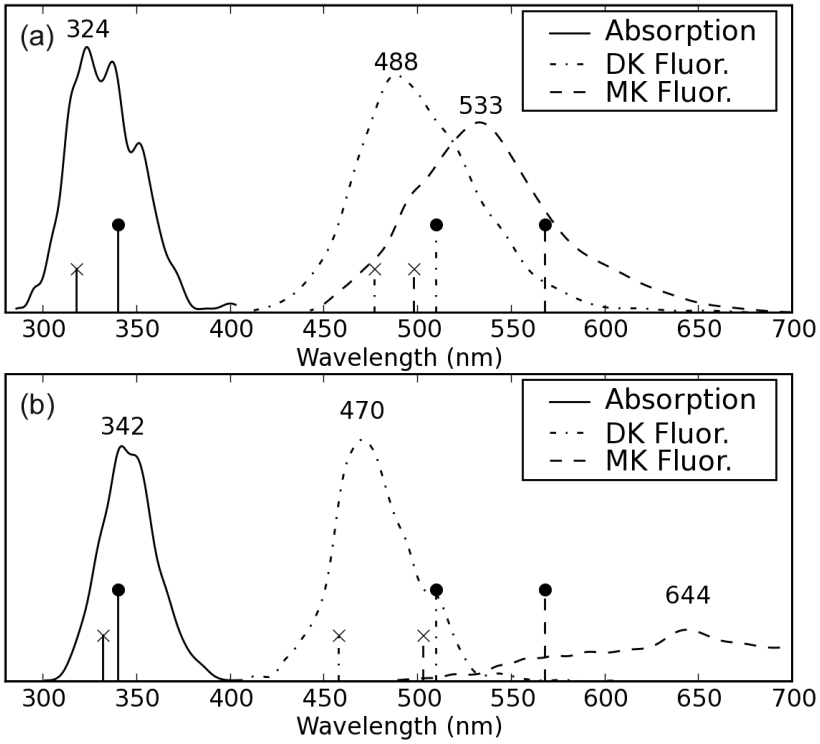

Figure 4.5: *Simulated absorption and emission spectra at the (a) RI-CC2/SVP-SV and (b) B3LYP/SVP-SV levels. Cirles show experimental band maxima [14], crosses vertical absorption and fluorescence energies respectively.*

both cases there is a ridge that should favor MK formation unless the starting conditions are highly symmetrical.

In Fig. 4.6 the time evolution of the DE, MK, and DK species (as defined in Eqns 3.3-3.5) is presented for dynamics simulations at the RI-CC2/SVP-SV and TDDFT/B3LYP/SVP-SV levels. In both cases a rapid drop of the initial DE population and formation of MK is observed. With RI-CC2 transfers start after just 3 fs, and 90% conversion is reached after 18.5 fs. The MK population shows a maximum at about 30 fs and subsequently more DK is formed. At 60 fs a small amount of the DE reappears. This result can be compared to a fluorescence anisotopy study [18] where a 350 fs decay component was observed when probing at 460 nm emission wave length. The signal was attributed to the DE form. The simulations indicate that these molecules do not stay in the Franck-Condon region for the whole time but rather that part of the wave packet is reflected back. After 100 fs 63% MK and 37% DK are present.

The results are quite different in the TDDFT dynamics. An initial rapid DE drop is observed but it is considerably slower and the time for 90% conversion is 42.5 fs which is more than twice the RI-CC2 value. Hardly DK formation is observed and after 100 fs only 5% DK are present. The difference can be attributed to the fact that MK is 0.1 eV lower in energy than DK at the TDDFT/B3LYP, that the barrier is higher than with RI-CC2, and that there is less excess energy from the vertical excitation (cf. Fig. 4.2).

The experiment[3] clearly shows that significant amounts of DK are present after 100 fs. This is in contradiction to the TDDFT results which will be not considered further. A problem with both methods is that the predicted transfer time is about a fifth of the 50 fs that were concluded from the experiment[3]. It is not clear wether this is a problem of the experimental interpretation or a computational inaccuracy. On the one hand it should be difficult to probe a 50 fs process with the 30 fs time resolution that was available. On the other hand the comparison between RI-CC2 and TDDFT dynamics also shows how small differences in the computation strongly affect the outcome. A close connection between both experiment and theory is needed to understand these open questions better.

It was almost always observed that DK formation proceeded with MK as a

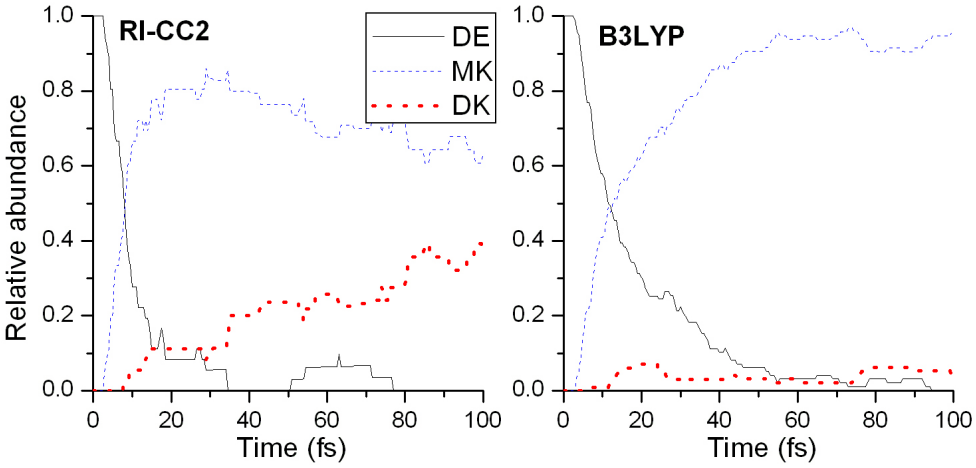

Figure 4.6: *Relative abundances of the DE, MK, and DK species over time for dynamics simulations at the RI-CC2/SVP-SV and TDDFT/B3LYP/SVP-SV levels.*

short term intermediate. This can be seen by projecting the dynamics onto the $\Delta R_1/\Delta R_2$ surface (Fig. 4.7). Both the DE-MK and the MK-DK paths are well populated and reactions take place in both directions. Only 2 trajectories are found on the symmetric DE-DK path. On average 2.0 proton transfers (cf. Sec. 3.4) were observed per trajectory in the first 100 fs: 1.2 $DE \rightarrow MK$, 0.5 $MK \rightarrow DK$, 0.2 $DK \rightarrow MK$, 0.2 $MK \rightarrow DE$. This gives the picture of a highly dynamical system rather than two separated reaction branches. This is in accordance with the relaxed PES presented above (Fig. 4.3) which makes it plausible that trajectories would slide off the ridge to form the MK rather than proceed in the symmetric process. But this picture is contrary to the prevalent experimtal interpretation [15, 3] which considers two branched isolated reaction channels and a one-directional $MK \rightarrow DK$ conversion on a 10 ps time scale. The question will be adressed in more detail below.

It is well documented in the literature that skeletal motions are decisive for the excited-state proton transfer [9, 6, 10, 11]. The acceptor and donor atoms have to move close enough together for the transfer to take place. To represent this movement the average value of the distance between the O and N atoms $R_{NO,active}$ involved in the process can be plotted against the reaction coordinate ΔR_{active}. It was shown that for the rigid 10-hydroxybenzo[h]quinoline

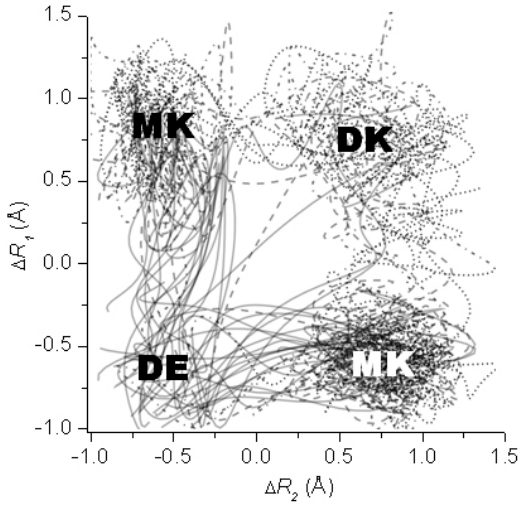

Figure 4.7: *Projection of the RI-CC2 trajectories onto the $\Delta R_1/\Delta R_2$ surface. Time coding: — 0-25 fs, - - - 25-50 fs, — · — · — 50-75 fs, ··· 75-100 fs*

molecule (HBQ) $R_{NO,active}$ decreases only by about 0.03 Å with the proton transfer whereas it is shortened by about 0.13 Å in the more flexible 2-(2'-hydroxyphenyl-)benzothiazole (HBT). This analysis for $BP(OH)_2$ is shown in Fig. 4.8. The NO distance when the trajectory starts is on average already 0.03 Å shorter than the equilibrium value. This can be understood by the fact that with the random initial conditions (cf. Sec. 3.1) the side with the shorter NO distance is favored to become the active side of the first proton transfer. In the course of the remaining process the NO distance shortens by only 0.02 more Å in connection with the transfer. After that the NO distance stretches as the molecule bends to the other side. The transfer proceeds very quickly (7 fs) compared to the HBT (36 fs)[11] and HBQ (30 fs)[10] dynamics simulations. The reason for this is probably that there is a competitive advantage with two proton transfer sites. Moreover there is a steep energy gradient for the first transfer. Whereas the experiment is very well in accordance with the simulations for HBT and HBQ, it gives a much longer time of about 50 fs[3] for the transfer in $BP(OH)_2$. To get some more insight on the problem, a symmetric trajectory starting from the undistorted C_{2h} ground state minimum with no initial momentum was run. In this case the symmetric concerted transfer occurs after 39 fs accompanied by an

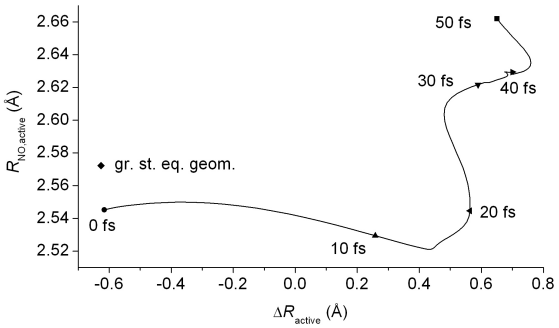

Figure 4.8: *Time dependence of the average NO distance $R_{NO,active}$ plotted against the average value of the reaction coordinate ΔR_{active}.*

NO contraction of 0.14 Å. This shows how strongly the process is either facilitated by the symmetry-breaking or the initial kinetic energy. The result emphasizes the multidimensional and dynamic nature of the process.

In the Fourier transform of the experimental transient three oscillations were seen. These were assigned to two totally symmetric modes ($21a_g, 20a_g$) and one antisymmetric mode ($20b_u$).[3] The corresponding motions in the DK ($S_1, \pi\pi^*$) are shown in Fig. 4.9. Similar motions where also found for the other tautomers. It can be seen that the $21a_g$ (and $20a_g$) modes shorten the O-N distances simultaneously whereas the $20b_u$ favors only one side in each half cycle. Therefore the totally symmetric modes were taken as evidence for a symmetric double transfer whereas the $20b_u$ motion could give a single transfer.[3]

It is interesting to consider that excitation of a non-totally symmetric mode in an allowed transition is against the Franck-Condon rules. The fact that it is observed is a direct evidence of the reactive process[3] and related to the strongly anharmonic potential. The precise formulation is that only even vibrational states of a non-totally symmetric mode can be accessed. This comes from the fact that the potential curves are symmetric because motion in both directions has to be equivalent. A significant excitation only occurs if the shape of the PES strongly changes with the electronic excitation.[57] This is the case in a reactive potential as observed here.

To compare with experimental results, standard deviations of normal mode mo-

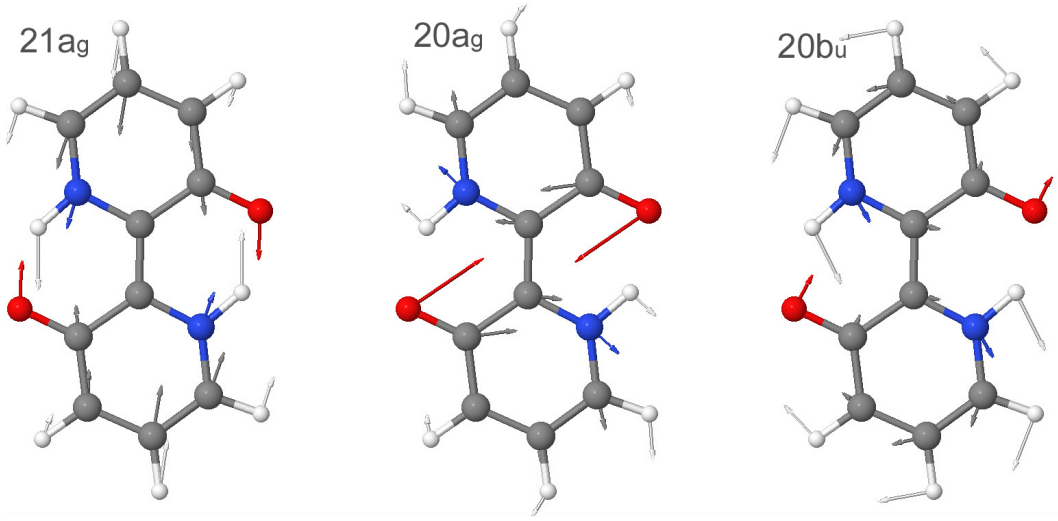

Figure 4.9: *Normal mode motions of the DK computed at the RI-CC2/SVP-SV level for the $S_1(\pi\pi^*)$ state.*

tions with respect to the DK reference geometry have been analyzed (cf. Sec. 2.3.4). The total ($\hat{\mathcal{R}}_{tot}$) and coherent ($\hat{\mathcal{R}}_{coh}$) standard deviations of the 24 lowest energy normal modes are presented In Fig. 4.10. $\hat{\mathcal{R}}_{tot}$ (light blue) represents total fluctuations and has a strong component for every mode. The magnitude should be mostly related to the initial condition sampling (Sec. 3.1). It is stronger for the looser low frequency modes. When averaging over trajectories is performed to produce $\hat{\mathcal{R}}_{tot}$, random motions should cancel out and only coherent motions that were caused by the electronic excitation should remain. In the part that can be sampled by a 30 fs experiment - below 550/cm (cf. 2.5) - just the three modes are found that were also mentioned there[3]. In the higher frequency range, three more modes are found. Particularly strong coherent behavior was found for $17a_g$ which is an aromatic breathing vibration. Its excitation is connected to a losening of the ring as an electron is excited from a bonding π-orbital to an anti-bonding π^*-orbital. Similar effects are known for other aromatic systems.

An important result of this analysis is that strong coherent activity of symmetric modes is not in contradiction to the symmetry breaking process that was observed. This can be understood by the fact that the superposition of a symmetric and an antisymmetric mode will yield an asymmetric motion. Activity of the symmetric mode was taken as a main argument for a symmetric reaction

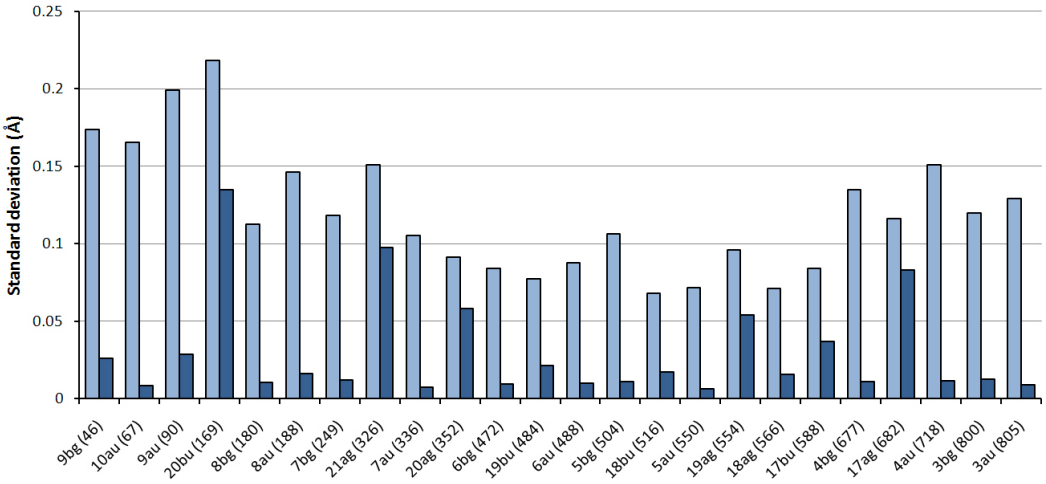

Figure 4.10: *Total ($\hat{\mathcal{R}}_{tot}$, light blue) and coherent ($\hat{\mathcal{R}}_{coh}$, dark blue) normal mode activity during the dynamics simulation as measured by the standard deviation of averaged displacement vectors with respect to the DK reference geometry. Vibrational frequencies are given in parentheses (cm^{-1}).*

path[3]. The analysis just performed relativizes this result and shows that the asymmetric process is consistent with experiment.

Chapter 5

Conclusions and Outlook

The excited state double proton transfer in [2,2'-bipyridyl]-3,3'-diol ($BP(OH)_2$) was examined by extended quantum chemical computations with the ab-initio RI-CC2 and TDDFT methods. First, benchmark computations on the surface of the first singlet excited state were performed to understand the physics of the molecule and test the consistency of the methods. Then ab-initio dynamics simulations considering all degrees of freedom were performed to follow the actual proton transfer process. The results were compared against experimental data to judge their accuracy.

Main attention was given to the question of sequential versus concerted proton transfer. The prevalent experimental interpretation[15, 3] considered a branched reaction path with a uni-directional $MK \rightarrow DK$ conversion on a 10 ps time scale. The simulations shed a completely new light on the process. It was found that MK and DK were readily interconverted in both directions during the 300 fs simulated. It was shown by considering the time-dependent spectra and particularly the normal mode oscillations that this highly dynamic rather than branched system is still in agreement with experimental results. The reaction scheme obtained from the dynamics simulations is shown in Fig. 5.1. The first transfer occured in 7 fs on average. After 30 fs a maximum of the MK intermediate was observed and enhanced DK formation proceeded. The direct symmetric $DE \rightarrow DK$ path was almost never observed. In the highly energetic system both reverse reactions: $DK \rightarrow MK$ and $MK \rightarrow DE$ took place. This outcome is opposed to the current

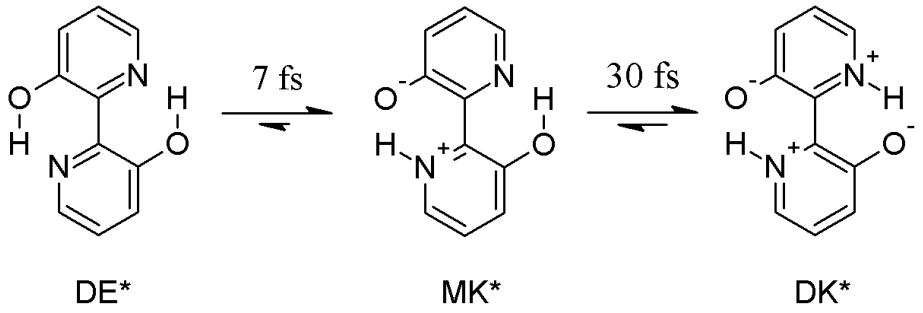

Figure 5.1: *Reaction scheme of the excited state intramolecular double proton transfer of $BP(OH)_2$ as concluded from the dynamics simulations in this work.*

experimental interpretation but in agreement with the epxerimental data. New experiments guided by these results may be able to either verify or disprove them and complete the understanding of $BP(OH)_2$ and other similar systems.

With the ever increasing speed of computers ab-initio computations of many molecules of technological and biological interest have become possible. More and more advanced probing techniques allow for the investigation of chemical processes on the atomic time and length scales. The advantage of the experimental approach is that the results are in essence correct. The downside is that the information is often indirect and difficult to interpret. Computation is the complimentary approach. On the one hand it gives direct insight into the simulated processes. On the other hand every kind of mathematical model necessitates coarsening as far as the surroundings, the physics, and the numerical approach are concerned (i.e. one does not have the analytical solution of the theory of everything for the whole universe). Therefore a computational solution will never yield a result with complete accuracy. As it was also noticed in this project it is the interplay between experiment and theory that gives a deeper insight into the physical and chemical processes surrounding us and allows for new developments in medicine and technology.

Acknowledgements

First I would like to thank my advisor Prof. Hans Lischka who was very supportive from the beginning on. Right after I had just done a three week internship in September 2007 I was sent to my first symposium where I could get to know the group and get a first glimpse of the field. Hans Lischka then gave me the chance to work on my thesis in parallel to my courses. This gave me the possibility to finish in due time and to work on some other interesting projects. I am grateful that I could deepen my understanding on five conferences and that I had the chance to go abroad four times during those one and a half years.

I would like to thank Dr. Mario Barbatti who closely supervised my project and helped me get familiar with the programs used. He also helped me to put the thesis into this final version. Thanks also to Dr. Adelia Aquino, Dr. Jaroslaw Szymczak, Dr. Daniel Tunega, Mag. Matthias Ruckenbauer, Mag. Hasan Pasalic, and Mag. Bernahrd Sellner. All of them were very supportive to help with all the tasks that came up during my thesis: usage of the quantum chemical programs, getting familiar with UNIX, keeping the computers running and so on. And thanks for many interesting disussions.

Thanks to my family and thanks to everyone who showed some interest in the project. It was always nice to talk about this work. And of course thanks to my parents for supporting me during my university time.

I acknowledge FWF funding that I received for a part of the time.

Deutsche Zusammenfassung

In dieser Arbeit wurde die Photochemie des [2,2'-Bipyridyl-]-3,3'-diol ($BP(OH)_2$) Moleküls untersucht (vgl. Fig. 1.2). $BP(OH)_2$ ist interessant wegen vieler möglicher Anwendungen des Moleküls und dessen Derivaten: zum Beispiel als LASER Farbstoff[13] als biochemische Sonde[22], als Photostabilisator oder Sonnenkollektor [17] oder aber auch im Zusammenhang von Kontrolltheorie[3]. Das Molekül besitzt zwei intramolekulare Wasserstoffbrücken, entlang derer nach UV Anregung die Wasserstoffatome transferiert werden. Experimente[13, 14, 15, 16, 17, 18, 3] und frühere Rechnungen[19, 20, 21, 5] haben den prinzipiellen Prozess dargelegt: Im Grundzustand ist die di-enol (DE) Form stabil, bei der beide Wasserstoffe an die Sauerstoffatome gebunden sind. Nach Anregung durch UV Licht werden innerhalb von 100 fs ein oder zwei Protonen transferiert und beide weiteren Tautomere, mono-keto (MK) und di-keto (DK) sind zu sehen.[18, 3] Mit einer Zeitkonstante von 10 ps wandelt sich dann MK in DK um.[15] Nach dem Transfer werden charakteristische Anregungen von Normalschwingungen beobachtet.[3] Schließlich fluoresziert das DK Tautomer. Einige Fragen sind aber noch nicht geklärt. Vor allem über den ersten Transferschritt ist wenig Information vorhanden, da dieser unter der experimentellen Zeitauflösung stattfindet.

Das Ziel des Projektes war es, den beschriebenen Prozess und dabei vor allem den ersten Transferschritt besser zu verstehen. Dafür wurde eine Molekulardynamiksimulation über die ersten 100 fs durchgeführt. Es wurde mit klassischen Kernen gerechnet, die sich im effektiven Feld der quantenmechanisch beschriebenen Elektronen bewegten. Die Elektronen im angeregten Zustand wurden mit den ab-initio Methoden der zeit-abhängigen Dichtefunktionaltheorie und "resolution of the identity second-order coupled cluster" gerechnet. Neben diesen Dynamikrechnungen wurden Teile der Energiefläche, insbesondere die stationären

Punkte, genauer untersucht und außerdem die Absorptions- und Fluoreszenzspektren simuliert.

Die Ergebnisse sind in Refs [55, 56] zu publiziert. In allen Trajektorien der Dynamiksimulation fanden Protonentransfers innerhalb der 100 fs nach UV Anregung statt, wobei MK und DK gebildet wurden. DK entstand allerdings fast ausschließlich über sequentielle Transfers mit MK als Zwischenprodukt. Dies ist im Gegensatz zur vorherrschenden experimentellen Interpretation[15, 3]. Dort wurde von einem verzweigten Reaktionsweg ausgegangen, in dem in einem ersten Schritt entweder MK oder direkt DK in einem symmetrischen Prozess gebildet wird. Es ist ein interessantes Resultat, das experimentell schwierig zugänglich war, dass der Prozess dynamischer ist, als bisher gedacht und keine zwei getrennten Reaktionswege vorliegen. Die Tatsache, dass auch dieser Ablauf mit den experimentellen Daten zusammenpasst, wurde genau überprüft. Insbesondere konnten auch die beobachteten Normalschwingungen reproduziert werden. Für diese Normalschwingungsanalyse wurden Python Routinen programmiert, die in das Newton-X Molukulardynamikpackage[26] integriert werden.

In dem Projekt konnte gesehen werden, wie mit modernen Simulationsmethoden ein chemischer Prozess direkt simuliert werden kann. Durch dass Zusammenspiel von Experiment und Rechnung war es auch in diesem Fall möglich, ein genaues Verständnis der Reaktion zu bekommen. Die Resultate sind einerseits im Hinblick auf die möglichen Anwendungen interessant. Andererseits helfen derartige Studien, das Verständnis von molekularen Prozessen zu verbessern, die sowohl von der Zeit- als auch von der Größenskala her weit unter den Alltagserfahrung liegen und zur Zeit eine große Herausforderung für Experiment und Rechnung sind.

Bibliography

[1] A. H. Zewail, *Journal of Physical Chemistry A* **104**, 5660 (2000).

[2] L. Serrano-Andres and M. Merchan, *Journal of Molecular Structure-Theochem* **729**, 99 (2005).

[3] K. Stock, C. Schriever, S. Lochbrunner, and E. Riedle, *Chemical Physics* **349**, 197 (2008).

[4] A. L. Sobolewski, *Physical Chemistry Chemical Physics* **10**, 1243 (2008).

[5] J. M. Ortiz-Sanchez, R. Gelabert, M. Moreno, and J. M. Lluch, *Chemphyschem* **9**, 2068 (2008).

[6] J. D. Coe, B. G. Levine, and T. J. Martinez, *Journal of Physical Chemistry A* **111**, 11302 (2007).

[7] A. L. Sobolewski, W. Domcke, and C. Hattig, *Proceedings of the National Academy of Sciences of the United States of America* **102**, 17903 (2005).

[8] G. E. O. Borgstahl, D. R. Williams, and E. D. Getzoff, *Biochemistry* **34**, 6278 (1995).

[9] S. Lochbrunner, A. J. Wurzer, and E. Riedle, *Journal of Chemical Physics* **112**, 10699 (2000).

[10] C. Schriever, M. Barbatti, K. Stock, A. J. A. Aquino, D. Tunega, S. Lochbrunner, E. Riedle, R. de Vivie-Riedle, and H. Lischka, *Chemical Physics* **347**, 446 (2008).

[11] M. Barbatti, A. J. A. Aquino, H. Lischka, C. Schriever, S. Lochbrunner, and E. Riedle, *Physical Chemistry Chemical Physics* **11**, 1406 (2009).

[12] A. Douhal, F. Lahmani, and A. H. Zewail, *Chemical Physics* **207**, 477 (1996).

[13] J. Sepiol, H. Bulska, and A. Grabowska, *Chemical Physics Letters* **140**, 607 (1987).

[14] H. Zhang, P. vanderMeulen, and M. Glasbeek, *Chemical Physics Letters* **253**, 97 (1996).

[15] D. Marks, P. Prosposito, H. Zhang, and M. Glasbeek, *Chemical Physics Letters* **289**, 535 (1998).

[16] F. V. R. Neuwahl, P. Foggi, and R. G. Brown, *Chemical Physics Letters* **319**, 157 (2000).

[17] L. Kaczmarek, P. Borowicz, and A. Grabowska, *Journal of Photochemistry and Photobiology a-Chemistry* **138**, 159 (2001).

[18] P. Toele, H. Zhang, and M. Glasbeek, *Journal of Physical Chemistry A* **106**, 3651 (2002).

[19] A. L. Sobolewski and L. Adamowicz, *Chemical Physics Letters* **252**, 33 (1996).

[20] V. Barone, A. Palma, and N. Sanna, *Chemical Physics Letters* **381**, 451 (2003).

[21] R. Gelabert, M. Moreno, and J. M. Lluch, *Chemphyschem* **5**, 1372 (2004).

[22] O. K. Abou-Zied, *Journal of Photochemistry and Photobiology a-Chemistry* **182**, 192 (2006).

[23] G. A. Worth and L. S. Cederbaum, *Annual Review of Physical Chemistry* **55**, 127 (2004).

[24] L. Verlet, *Phys. Rev.* **159**, 98 (1967).

[25] J. C. Tully, *Faraday Discussions* , 407 (1998).

[26] M. Barbatti, G. Granucci, M. Persico, M. Ruckenbauer, M. Vazdar, M. Eckert-Maksic, and H. Lischka, *Journal of Photochemistry and Photobiology a-Chemistry* **190**, 228 (2007).

[27] M. Ben-Nun, J. Quenneville, and T. J. Martinez, *J. Phys. Chem. A* **104**, 5161 (2000).

[28] C. F. F. Karney, *Journal of Molecular Graphics and Modelling* **25**, 595 (2007).

[29] L. Kurtz, A. Hofmann, and R. de Vivie-Riedle, *Journal of Chemical Physics* **114**, 6151 (2001).

[30] A. Amadei, A. B. M. Linssen, and H. J. C. Berendsen, *Proteins-Structure Function and Genetics* **17**, 412 (1993).

[31] A. Szabo and N. S. Ostlund, *Modern Quantum Chemistry*, MacGraw-Hill, Inc., 1989.

[32] C. Hättig, Electronic Structure: Hartree-Fock and Correlation Methods, in *Multiscale Simulation Methods in Molecular Sciences, Lecture Notes*, edited by J. Grotendorst, A. Attig, S. Bügel, and D. Marx, Jülich Supercomputing Centre, 2009.

[33] F. Weigend and M. Haser, *Theoretical Chemistry Accounts* **97**, 331 (1997).

[34] O. Christiansen, H. Koch, and P. Jorgensen, *Chemical Physics Letters* **243**, 409 (1995).

[35] P. Hohenberg and W. Kohn, *Physical Review B* **136**, B864 (1964).

[36] R. G. Parr and W. Yang, *Density-Functional Theory of Atoms and Molecules*, Oxford University Press, 1989.

[37] W. Kohn and L. J. Sham, *Physical Review* **140**, 1133 (1965).

[38] R. Zeller, Density Functional Theory and Linear Scaling, in *Multiscale Simulation Methods in Molecular Sciences, Lecture Notes*, edited by J. Grotendorst, A. Attig, S. Bügel, and D. Marx, Jülich Supercomputing Centre, 2009.

[39] M. Merchan and L. Serrano-Andres, Ab Initio Methods for Excited States, in *Computational Photochemistry*, edited by M. Olivucci, Elsevier, 2005.

[40] F. Furche and D. Rappoport, Density Functional Methods for Excited States: Equilibrium Structure and Electronic Spectra, in *Computational Photochemistry*, edited by M. Olivucci, Elsevier, 2005.

[41] M. S. de Vries and P. Hobza, *Annual Review of Physical Chemistry* **58**, 585 (2007).

[42] A. Douhal, S. K. Kim, and A. H. Zewail, *Nature* **378**, 260 (1995).

[43] D. R. Borst, J. R. Roscioli, D. W. Pratt, G. M. Florio, T. S. Zwier, A. Muller, and S. Leutwyler, *Chemical Physics* **283**, 341 (2002).

[44] L. Serrano-Andres and M. Merchan, *Chemical Physics Letters* **418**, 569 (2006).

[45] S. Lochbrunner, K. Stock, C. Schriever, and E. Riedle, Symmetry breaking wavepacket motion and absence of deuterium isotope effect in ultrafast excited state proton transfer, in *Femtochemistry and Femtobiology*, edited by M. Martin and J. Hynes, Elsevier, 2004.

[46] S. Grimme, F. Furche, and R. Ahlrichs, *Chem. Phys. Lett.* **361**, 321 (2002).

[47] R. Bauernschmitt and R. Ahlrichs, *Chem. Phys. Lett.* **256**, 454 (1996).

[48] C. Hattig and F. Weigend, *J. Chem. Phys.* **113**, 5154 (2000).

[49] C. Hattig and A. Kohn, *J. Chem. Phys.* **117**, 6939 (2002).

[50] A. D. Becke, *Journal of Chemical Physics* **98**, 1372 (1993).

[51] A. J. A. Aquino, H. Lischka, and C. Hattig, *Journal of Physical Chemistry A* **109**, 3201 (2005).

[52] R. Ahlrichs, M. Bar, M. Haser, H. Horn, and C. Kolmel, *Chem. Phys. Lett.* **162**, 165 (1989).

[53] A. Schafer, C. Huber, and R. Ahlrichs, *Journal of Chemical Physics* **100**, 5829 (1994).

[54] A. Schafer, H. Horn, and R. Ahlrichs, *J. Chem. Phys.* **97**, 2571 (1992).

[55] F. Plasser, M. Barbatti, A. J. A. Aquino, and H. Lischka, **submitted** (2009).

[56] A. J. A. Aquino, F. Plasser, M. Barbatti, and H. Lischka, *Croatica Chemica Acta* **in print** (2009).

[57] F. Negri and G. Orlandi, Electronic and Vibronic Spectra of Molecular Systems: Models and Simulations based on Quantum Chemically Computed Molecular Parameters, in *Computational Photochemistry*, edited by M. Olivucci, Elsevier, 2005.

List of Tables

4.1 Lengths of the hydrogen bonds computed with different methods. Optimizations were done with C_s restriction. FC denotes Franck-Condon structure, i.e. the ground state DE. MK and DK are optimized in the $S_1(\pi\pi^*)$ state. 35

4.2 Vertical excitation and fluorescence energies (eV) of the first singlet excited states computed at different levels of theory. Oscillator strengths are shown in parentheses. 38

List of Figures

1.1 General scheme of ESIPT: The stable tautomer in the ground state (where the hydrogen is often localized on an oxygen) is referred to here as enol (E). After UV excitation the proton transfer to keto (K*) proceeds. K* relaxes either by emitting light with a strong Stokes shift or by internal conversion (IC). 2

1.2 The three tautomers of the [2,2'-bipyridyl-]-3,3'-diol molecule: di-enol (DE), mono-keto (MK), di-keto (DK) 4

4.1 Ground state (DE) and S_1 ($\pi\pi^*$) state (MK, DK) fully optimized geometries at the RI-CC2/SVP-SV level. (TD)DFT/B3LYP/TZVP values are shown in parentheses; at the MK the TDDFT/B3LYP/TZVP structure with planarity restriction is taken as no true local MK minimum was found. For DE and DK only symmetry unique values are shown. DE and DK are planar, MK shows an NCCN interring torsion angle of 175°. 36

4.2 S_1 ($\pi\pi^*$) energies for planar structures relative to the DE ground state minimum computed at the RI-CC2 and TDDFT/B3LYP levels using the SVP-SV and TZVP basis sets, TZVP results in parentheses. 37

4.3 Relaxed PES with fixed OH-distances under planarity constriction in the $\pi\pi^*$ state computed at the RI-CC2/SVP-SV (a) and TDDFT/B3LYP/SVP (b) levels. 39

4.4 Linear PES computed at the RI-CC2/TZVP (a) and TDDFT/B3LYP/TZVP (b) levels. The structures were constructed according to (3.1). . . 40

4.5 Simulated absorption and emission spectra at the (a) RI-CC2/SVP-SV and (b) B3LYP/SVP-SV levels. Cirles show experimental band maxima [14], crosses vertical absorption and fluorescence energies respectively. 42

4.6 Relative abundances of the DE, MK, and DK species over time for dynamics simulations at the RI-CC2/SVP-SV and TDDFT/B3LYP/SVP-SV levels. 44

4.7 Projection of the RI-CC2 trajectories onto the $\Delta R_1/\Delta R_2$ surface. Time coding: $-$ 0-25 fs, - - - 25-50 fs, $-\cdot-\cdot-$ 50-75 fs, $\cdots$ 75-100 fs 45

4.8 Time dependence of the average NO distance $R_{NO,active}$ plotted against the average value of the reaction coordinate ΔR_{active}. . . . 46

4.9 Normal mode motions of the DK computed at the RI-CC2/SVP-SV level for the $S_1(\pi\pi^*)$ state. 47

4.10 Total ($\hat{\mathcal{R}}_{tot}$, light blue) and coherent ($\hat{\mathcal{R}}_{coh}$, dark blue) normal mode activity during the dynamics simulation as measured by the standard deviation of averaged displacement vectors with respect to the DK reference geometry. Vibrational frequencies are given in parentheses (cm^{-1}). 48

5.1 Reaction scheme of the excited state intramolecular double proton transfer of $BP(OH)_2$ as concluded from the dynamics simulations in this work. 50